April 2016

Manta Ray Robot

Gabrielle Helene Franzini
Worcester Polytechnic Institute

John Holland Price
Worcester Polytechnic Institute

Joshua Francis Fuller
Worcester Polytechnic Institute

Nathan Schmidt
Worcester Polytechnic Institute

MANTA RAY ROBOT

A Major Qualifying Project Submitted
to the Faculty of Worcester Polytechnic Institute
in partial fulfillment of the requirements for the
Degree in Bachelor of Science in
Robotics & Mechanical Engineering
By:

Gabrielle Franzini

Joshua Fuller

John Price

Nathan Schmidt

Date: 5/1/16
Project Advisor:

Professor Susan Jarvis

Abstract

The goal of this project was to improve UAV efficiency through use of biomimetic design. This was achieved through the application of a hydraulically actuated soft robotic fin. Drawing inspiration from the manta ray, a custom actuator was developed to achieve a feasible, lifelike locomotion method. The actuator was incorporated into a prototype robot to assess the performance and ease of integration.

Oceanic Manta Ray [1]

[1] (Hanson, 2005)

Table of Contents

1.0 Introduction

Exploration of the oceans is not a simple task, requiring specialized technology. One such technology is AUVs, or Autonomous Underwater Vehicles which are "robotic vehicles that, depending on their design, can drift, drive, or glide through the ocean without real-time control by human operators".[2] AUVs have been built and programmed to perform a wide range of tasks, from mapping the ocean floor to monitoring environmental conditions. A variety of sensors can be used to gather data about different aspects of the environment. Control systems can also be employed to allow intelligent movement by an AUV so it can actively explore the area to which it travels.

Much of technology draws inspiration from nature, so much so that we have a term for it. Biomimetics, or biomimicry, is "the study and development of synthetic systems that mimic the formation, function, or structure of...biological mechanisms and processes".[3] Mimicking biology, especially in the case of animals, is beneficial particularly in the cases where the animal performs better than existing technology.[4] For instance, inspiration was taken from a gecko to create RiSE, a robot that can climb vertical surfaces.[5] Previously, navigating vertical terrain would have been very difficult.

There are some instances where inspiration from biology has been applied specifically to AUVs. For example, several types of robotic fish have been created focusing on mimicking different characteristics of movement. Tested motion patterns include lateral movement, complex movement of pectoral fins, tail motion, and other naturally adaptive processes that could be beneficial to an operating AUV. The mechanical movement is important, but it also needs to be controlled properly. In order to behave like a fish, the control systems should be able to adapt to changing environmental conditions based on input from the sensor systems. This could also contribute to the goal of navigation over a longer distance.[6] Another reason for exploring a biomimetic model is the potential for reduced energy cost at a

[2] (Autonomous Underwater Vehicles, 2015)

[3] (Biomimetic, 2015)

[4] (Fish & Kocak, 2011)

[5] (RiSE Project, 2015)

[6] (Du, Li, & Youcef-Toumi, 2015)

comparable performance level.[7] Fish can have a propulsion efficiency of up to 90%, while typical rotary propellers have about half of that.[8]

The project evaluated several actuation methods with respect to their use in biomimicry. Throughout several cycles of manufacturing, analysis, and revision, a soft robotic fin and the process for fabricating it were developed. An on-board power supply and microcontroller allowed the robot to operate untethered. Essential sensors provided feedback necessary for intelligent actuation.

This report discusses a basic background of Autonomous Underwater Vehicles and introduces some similar projects. Next, the progress and methodology of the project are described, including research, prototyping, manufacturing and testing. Lastly, results of the project are presented and areas for future work are suggested.

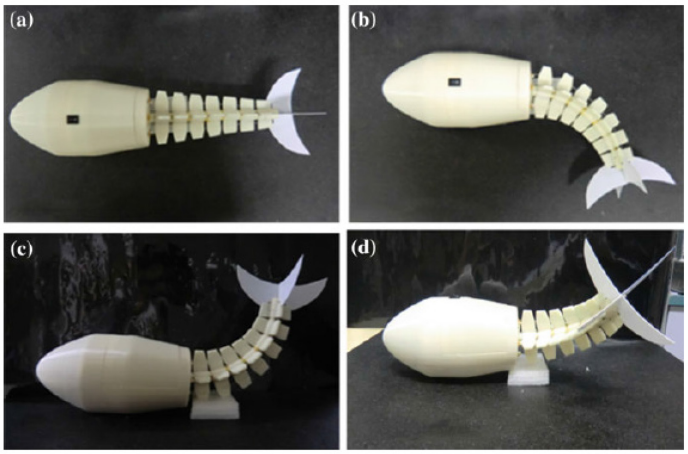

FIGURE 1: ROBOTIC FISH MIMICKING DOLPHIN AND SHARK MOVEMENT [9]

[7] (NASA Virginia Space Grant Consortium, 2015)

[8] (Du, Li, & Youcef-Toumi, 2015)

[9] (Du, Li, & Youcef-Toumi, 2015)

2.0 Background

2.1 History of AUVs

A major limiting factor to current AUVs is propulsion and energy efficiency. With the energy density of currently available power storage systems, AUVs are limited in their operating time. While gliders and floats generally require very little power to operate, these methods are not suitable when a higher degree of maneuverability is required. The most common alternative is the screw propeller found in many boats. MIT's maneuverable underwater vehicle Rex II[10], for example, is capable of fine motor control but is limited to 8 hours of operating time or 15 km while their Odyssey IV[11] is capable of roughly 11 hours or 80 km. Both of these vehicles utilize screw propeller propulsion.

There are some forms of underwater vehicles that can operate for long periods of time usually gathering data in various oceans at the cost of control and accuracy in its travel. For instance, sea gliders use changes in buoyancy to roughly control their trajectory in the water. This saves power, but as a result, the end destination can be difficult to calculate.

Another example of long term sea vehicles is Argo floats. These floats can stay in the water for over four years, gathering data and relaying it through satellites. The tradeoff of staying in the water so long is that they cannot be steered or navigated other than following the currents. They only adjust their buoyancy to gather data from deeper in the ocean and to reach the surface to relay their information.[12] These floats are ideal for mapping information about the ocean on a global scale, but they are not designed for gathering details for a specific area.

2.2 Biomimetics

In addition to the propulsion, other capabilities seen in nature can be applied to a bio-inspired underwater robot. For instance, quiet movement and maneuverability would allow for exploration into sensitive environments and areas that are difficult to navigate with traditional AUVs. A vehicle that

[10] (AUV Laboratory at MIT Sea Grant - REXII Flyer, 2015)

[11] (AUV Laboratory at MIT Sea Grant - Odyssey IV, 2015)

[12] (Argo Floats, 2015)

resembled an actual sea creature could be helpful in examining an environment without disturbing the existing wildlife.

There have been significant advances in artificial muscles and other actuation technologies. The potential advantages and disadvantages of the most promising biomimetic actuation methods were considered as shown in section 3.2: Actuation Comparison.

2.3 Similar Projects

This project is not the first of its kind. There have been numerous research studies into the movement of various rays and their efficiency. Additionally, there have been a number of notable manta ray robots. The most well-known being the Festo Aqua Ray, a small robot aiming to show off Festo's new actuators, allowing for no payload and with minimal information published on efficiency and cost.[13] The second notable project was a joint venture with the University of Virginia and the Department of the Navy. Although this robot is an amazing advancement, it relies on rigid structures, is not autonomous, and has poor energy efficiency.[14] Additionally, the soft robotic fish from WPI used sections of channels set into silicone that expand and bend when filled with a fluid. The result was a high degree of natural articulation. However they chose to use compressed air, which cannot be recompressed without significant power onboard, requiring air in the system be expelled to the outside water. This, in turn, gave the robot a limited finite operating capacity, as the number of actuations was limited by the amount of compressed air carried onboard.[15]

[13] (Festo Aqua Ray, 2015)

[14] (Mantabot, 2015)

[15] (Marchese, Onal, & Rus, 2014)

FIGURE 2: BIO-INSPIRED MANTABOT FROM UNIVERSITY OF VIRGINIA [16]

2.4 Project Goals

In order to create an AUV that has combined maneuverability and efficiency, it was decided to base the robot on the manta ray. Manta rays' oscillating propulsion allows for a reasonable degree of control while requiring less energy consumption than traditional methods. Additionally, their wide thin shape allows them to glide through the water while traveling over longer distances.

Goals were prioritize into a three tiered system. Tier 1 consisted of goals which the device needed to achieve in order to be considered a robot and for the project to be considered a success. This included autonomy so the robot could move on its own, untethered, to perform a pre-programmed mission. Another main goal was the oscillatory movement of the fins, out of the water, reminiscent of the movement performed by a manta ray.

Tier 2 goals were important to the development of the robot, but were not all required for the success of this iteration of the project. They were mainly focused on having the robot perform in the water. For instance waterproofing is necessary for it to operate as an underwater vehicle. Buoyancy control would allow the robot to dive and surface while directional control would allow it to turn as desired. To further mimic a manta ray, considerable speed and efficiency were desired when operating in the water. A fail safe system would prevent extensive damage or loss of components in the event of a

[16] (Mantabot [Digital Image], n.d.)

malfunction and a ping signal for recovery would simulate ability to locate the robot as if from a long mission.

Tier 3 goals were stretch goals known to be unlikely to be completed in full by this year's team. Instead, they point to future areas of interest that could further develop the result from this year's project. A more comprehensive surface location capability would allow for the robot to be tracked on the surface from a significant distance for recovery. Depth hardening would allow deeper parts of the ocean to be explored, and navigation under the surface would mean autonomous missions could be more effective. Lastly, 100% natural movement that biologically mimics a manta ray would create a robot of even greater speed and efficiency.

Tier 1	Tier 2	Tier 3
Basic Oscillatory Motion	Watertight	Surface Location Capabilities for Recovery
Untethered	Buoyancy Control	Depth Hardening
Fully Autonomous	Directional Control	Navigation
Environmentally Safe	Efficiency and Speed in Water	100% Natural Movement
	Fail Safe System	
	Ping Signal for Recovery	

FIGURE 3: PROJECT GOALS

3.0 Preliminary Designs & Prototyping

3.1 Initial Design Considerations

To begin the design process, the size of robot had to be decided. Matching the true scale of the adult oceanic manta ray was not an attainable goal since they generally achieve a 240in wingspan. Therefore, a small scale version with a wingspan of 66in was agreed upon. Using anatomical ratios shown in Figure 3.1.1, a body length of 33in was calculated. These dimensions led to a rigid body structure that is approximately 19in wide.

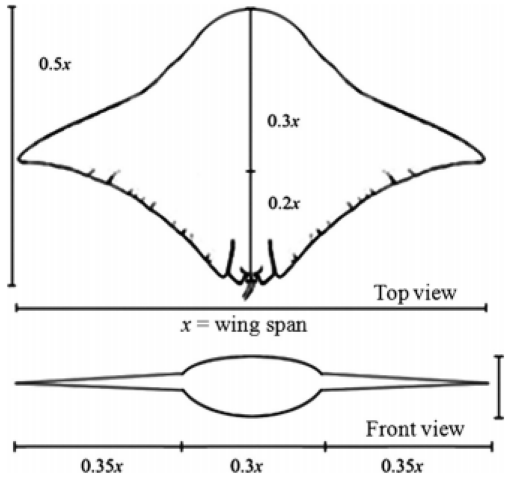

FIGURE 4: ANATOMICAL RATIOS [17]

The central "body" provided several necessary features for the robot. The first was acting as a watertight housing for the batteries, electronics, pumps, and valves that were be necessary for the robot's operation. The body is also a rigid structure that acts as the ground for the flapping mechanisms. The structure was initially designed in two pieces made up of a bottom tub and a detachable cover with a waterproof seal between the sections. This configuration would allow for easy access for internal assembly, maintenance, and battery exchange/charging. Initial considerations for building the chassis structure consisted of rapid prototyping, milling metal, or injection molding plastic.

[17] (Zhou & Low, 2011)

The initial design included the fins directly attached to each side of the rigid chassis structure. There were many options that needed to be considered, necessitating the implementation of some small prototypes, before the decision could be made for the hull structure and design of the fins.

3.2 Actuation Comparison

Actuation was highly important to the success of the project. Being able to achieve a functional range of motion with a reliable mechanism was paramount in achieving the project's goals. Desired actuation was based on the nature of the movement of actual manta rays. Achieving a similar magnitude of fin deflection, about 35 degrees, would provide the closest representation of the manta's motion.[18] Additionally, the design of the sub-systems depended on the method of actuation. Considerations for several types of actuation are explained in more detail below.

3.2.1 Electroactive Polymer Actuation

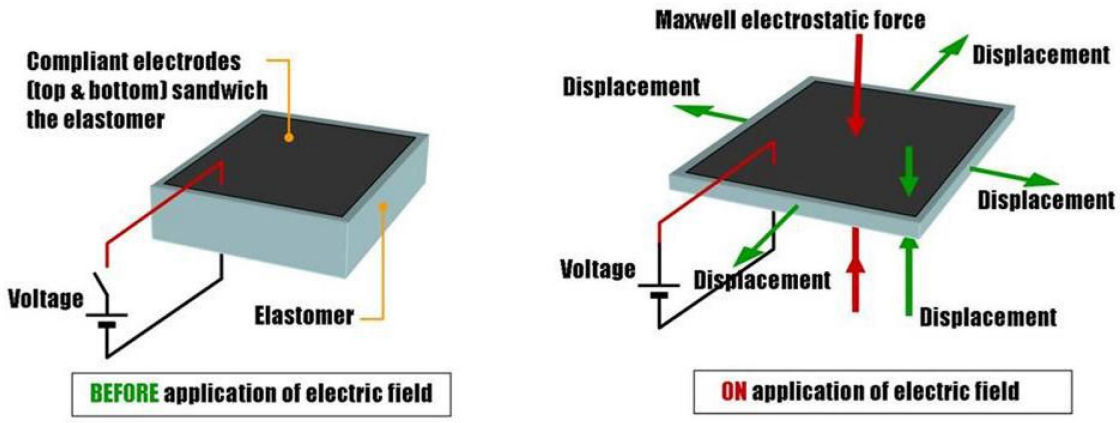

FIGURE 5: ELECTROACTIVE POLYMER [19]

Artificial muscles refers to use of an electroactive polymer that contracts when electricity is passed through it. One benefit to this method is that the actuation and assembly are one unit. This means the artificial muscle will reach the length of the fin as well as provide the mechanical force to move the fin. This combination results in fewer parts required for the system to function. However, this

[18] (Maia, Wilga, & Lauder, 2012)

[19] (Electroactive Polymer [Digital Image], n.d.)

technology is still relatively new and is prohibitively expensive. Furthermore, other biomimetic projects have cited the electroactive polymers as having a limited range of motion compared to other actuation systems.[20,21]

3.2.2 Conventional Hydraulic Actuation

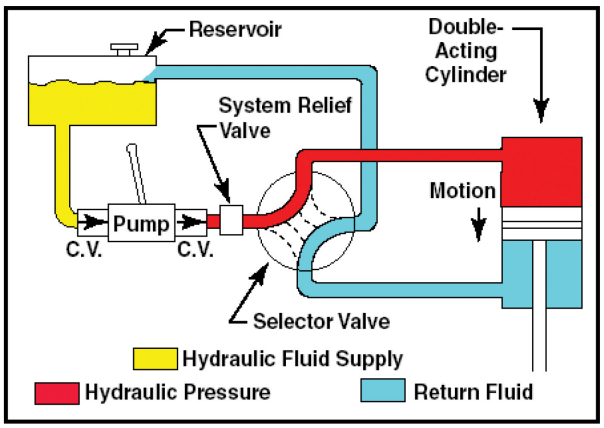

FIGURE 6: FLUID ACTUATION SYSTEM [22]

Fluid driven systems are often used in soft robotics. These systems involve pressurization of a cylinder to move a piston, which applies a force. These systems are generally very reliable and offer uniform loading. Additionally, pumps required for a fluid driven system can be selected for energy efficiency without sacrificing much function in the actuation system. However, due to limited space for the piston to move based on the cylinder's length, a fluidic system would have significantly limited range of motion.[23,24]

[20] (Huber, Fleck, & Ashby, 1965)

[21] (Electroactive Polymers | MIT Technology Review, 2002)

[22] (Hydraulic System [Digital Image], n.d.)

[23] (Huber, Fleck, & Ashby, 1965)

[24] (Bishop-Moser, Krishnan, Kim, & Kota, 2012)

3.2.3 Geometry Driven Actuation

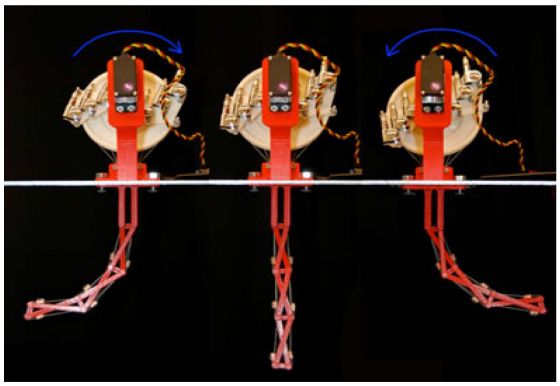

FIGURE 7: GEOMETRY DRIVEN ACTUATION [25]

Geometry driven systems use linkages and geometric structures to transfer loads. This allows for wide range of motion and complex motion depending on the configuration of the system. Although these systems are versatile, they can become very complex, making design and fabrication difficult. Additionally, many large geometry driven systems require multiple motors per assembly, making the energy cost relatively high.[26]

3.2.4 Wire Driven Actuation

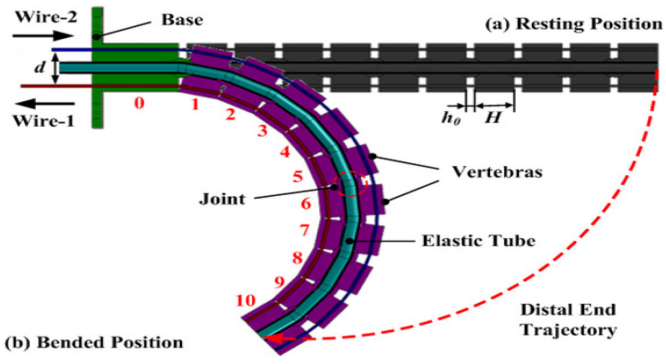

FIGURE 8: WIRE DRIVEN ACTUATION CROSS SECTION [27]

[25] (Geometric Actuation [Digital Image], n.d.)

[26] (Huber, Fleck, & Ashby, 1965)

[27] (Serpentine Wire Mechanism [Digital Image], n.d.)

Wire driven systems use inextensible cables to transfer force along the length of an assembly. These can be paired to offer directional control of the contraction on either side of an assembly, mimicking muscles. Due to space limitations, wire driven systems in submersibles have very limited motion, generally yielding basic two dimensional motion.[28]

3.2.5 PneuNet Actuation

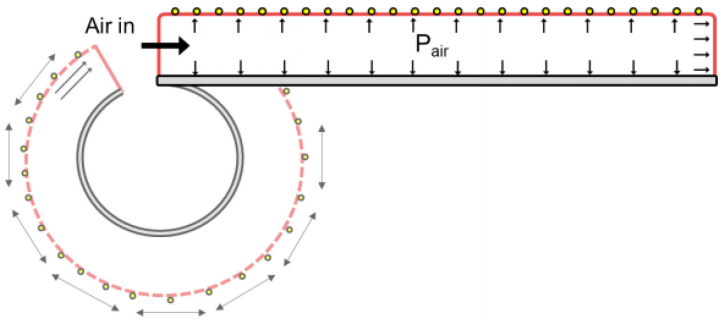

FIGURE 9: PNEUNET ACTUATION WITH RESTRICTED MOTION [29]

A pneumatic network (PneuNet) actuation system combines the concepts of geometry actuation and fluid driven actuation, allowing the pressurization of tubes or channels to work with geometric structures, yielding a hybrid method of actuation. This system allows a wide range of complex motion due to the ability of the geometric system to bend in multiple directions, and the ability of the fluid system to create equalized pressure throughout the actuation tubes. Fluid systems also use less energy than a mechanical system would, due to the reduced number of actuation devices needed per assembly.[30,31]

3.3 Preliminary Testing

In the decision matrix below, several actuation methods were scored according to whether they hindered, did not meet, met, or exceeded relevant criteria. Based on the results of that decision matrix,

[28] (Bishop-Moser, Krishnan, Kim, & Kota, 2012)

[29] (Harvard College, n.d.)

[30] (Huber, Fleck, & Ashby, 1965)

[31] (Bishop-Moser, Krishnan, Kim, & Kota, 2012)

two types of actuation were tested for possible implementation. The first was a fiber-reinforced elastomeric tube, derived from the work done by Bishop-Mosher et al.[32] This method was able to produce complex motions including bending and torsion, however, it was difficult to fabricate. The second method involved molding channels directly into the silicone fins. Rows of channels were molded along the top and a row along the bottom of the fin. The flapping motion was created by pressurizing either the top or bottom row of channels.[33]

[32] (Bishop-Moser, Krishnan, Kim, & Kota, 2012)

[33] (Marchese, Onal, & Rus, 2014)

	Weight	Artificial Muscles	Fluid Driven System	Geometry Driven System	Wire Driven System	Combination of Fluid and Geometry Driven System
Capable of Complex Motion	2	1	1	1	0	2
Range of Motion	2	0	1	1	0	2
Energy Efficient	2	2	1	1	0	1
Reliable (low failure rate)	1.5	2	1	2	1	1
Cost Effective	1	-1	1	1	2	1
Low Risk of Leaking	1	2	1	2	2	1
Proven Results	1	0	1	2	1	2
Unweighted Totals		6	7	10	6	**10**
Weighted Totals		10	10.5	14	6.5	**15.5**

Key: -1 - hinders criteria; 0 - does not meet criteria; 1 - meets criteria; 2 - exceeds criteria

FIGURE 10: PROPULSION SYSTEM DECISION MATRIX

3.3.1 Combinations of Fluid and Geometry Driven Systems

3.3.1.1 FIBER REINFORCED ELASTOMERIC TUBE SYSTEM

Fiber reinforced elastomeric tube actuation relies on the interaction between the expansion of the tube and the rigidity of the fiber surrounding it. As the tube expands horizontally, the fibers limit the movement of the tube in certain directions based on how it is configured. With proper design, exact motion can be achieved with this system.[34] Combining multiple tubes yields a larger range of complex motion. Multiple systems of these tubes in a sequence would theoretically have allowed for the motion desired for a manta ray fin.

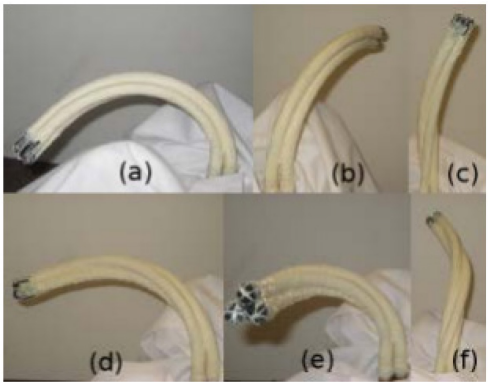

FIGURE 11: MULTI-ELASTOMER ACTUATION SYSTEM [35]

To implement fiber-reinforced elastomeric tubes, they would have needed to be pre-fabricated. The silicone fins would then be poured around the tubes. This guarantees the tubes to be perfectly fitted inside the fin, allowing all generated forces to be applied directly to the fin.[36]

Several of these actuators were fabricated using latex tubes wrapped with different configurations of sewing thread that were bonded using rubber cement. These tubes were difficult and time consuming to construct because the threads needed to be placed precisely. The prototypes were tested by pressurizing the tube with air from a bike pump. It was found that the prototypes had very limited and erratic motion. In addition, there were problems effectively sealing the free end of the

[34] (Fiber-Reinforced Actuators, 2015)

[35] (Bishop-Moser, Krishnan, Kim, & Kota, 2012)

[36] (Bishop-Moser, Krishnan, Kim, & Kota, 2012)

tubes. Ultimately, the complexity in the fiber placement, the length of the process and low output deflection made it impractical to move forward with this design.

3.1.2 SILICONE PNEUMATIC NETWORK BENDING SYSTEM

After the failures with the fiber reinforced elastomeric tube actuators, some more research was done for the pneumatic network bending system. One excellent resource was the Soft Robotics Toolkit, a well-respected Harvard research website.[37] This included many small scale example actuators that used the pneumatic network method, including step-by-step instructions for manufacturing them. The WPI Soft Robotic Fish paper was another useful resource that implemented this type of molded silicone actuator to create a successful biomimetic robot that mirrored the flexibility and movement of a fish.[38] Due to the similarities in application to the manta ray, this became the chosen type of actuator to move forward with in prototyping.

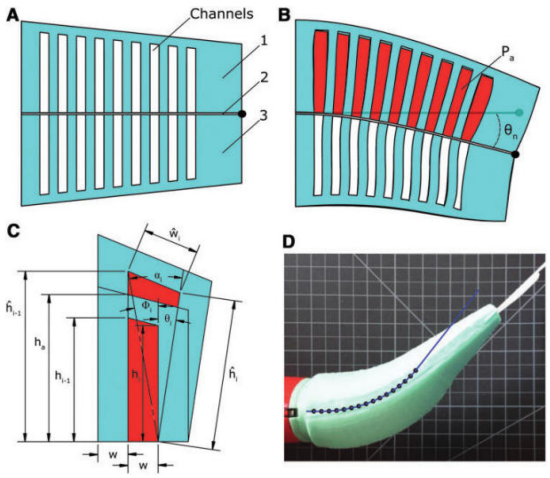

FIGURE 12: SOFT ROBOTIC FISH ACTUATION [39]

3.4 Small Scale Fin Prototypes

There were several iterations of small scale fin prototypes consisting of different designs and materials to determine which combination would be the best option for scaled prototyping and,

[37] (PneuNet Actuator, 2015)

[38] (Marchese, Onal, & Rus, 2014)

[39] (Soft Robotic Fish [Digital Image], n.d.)

ultimately, full sized fins. Some simple simulations were conducted in SolidWorks to try to predict the response. Later, these simulations were compared to the results of the small prototype tests to verify the validity of the models. Although initial simulations proved promising, more complex models resulted in large discrepancies between projections and actual results.

3.4.1 Full Fin - Oomoo

The first set of prototypes was modeled as a small scale full fin cast in silicone. Oomoo was the silicone chosen for the properties of 240 psi tensile strength and 250% elongation at break. The mold was created as a two part model in SolidWorks then 3D printed. The size of the mold allowed for a fin that was approximately ¼ scale of the final design choice.

The full fin mold had an open top to allow polystyrene foam channel inserts to be suspended in the mold and for the uncured silicone to be poured. The foam was carved by hand into two half cylinders and then wrapped in string to create strategic inextensibility as shown by the Fiber Reinforced Actuators in the Soft Robotics Toolkit.[40] The string wrapped around the outside of the foam was to prevent the channel from expanding outward in all directions, constraining deformations to the axial direction. Another set of strings lying against the flat face of the half cylinder in the root-to-tip direction created the inextensible layer across the chord line of the fin that would cause it to curl rather than stretch linearly. For this to actually be implemented, the foam channels were set in the silicone then melted out with acetone. The strings on the outside of the foam stayed embedded in the silicone to provide the structure for the movement once the channels were filled with fluid. The two channels for the small scale fin were placed on either side of a laterally oriented center plane to allow movement in both directions depending on which channel was filled.

[40] (Fiber-Reinforced Actuators, 2015)

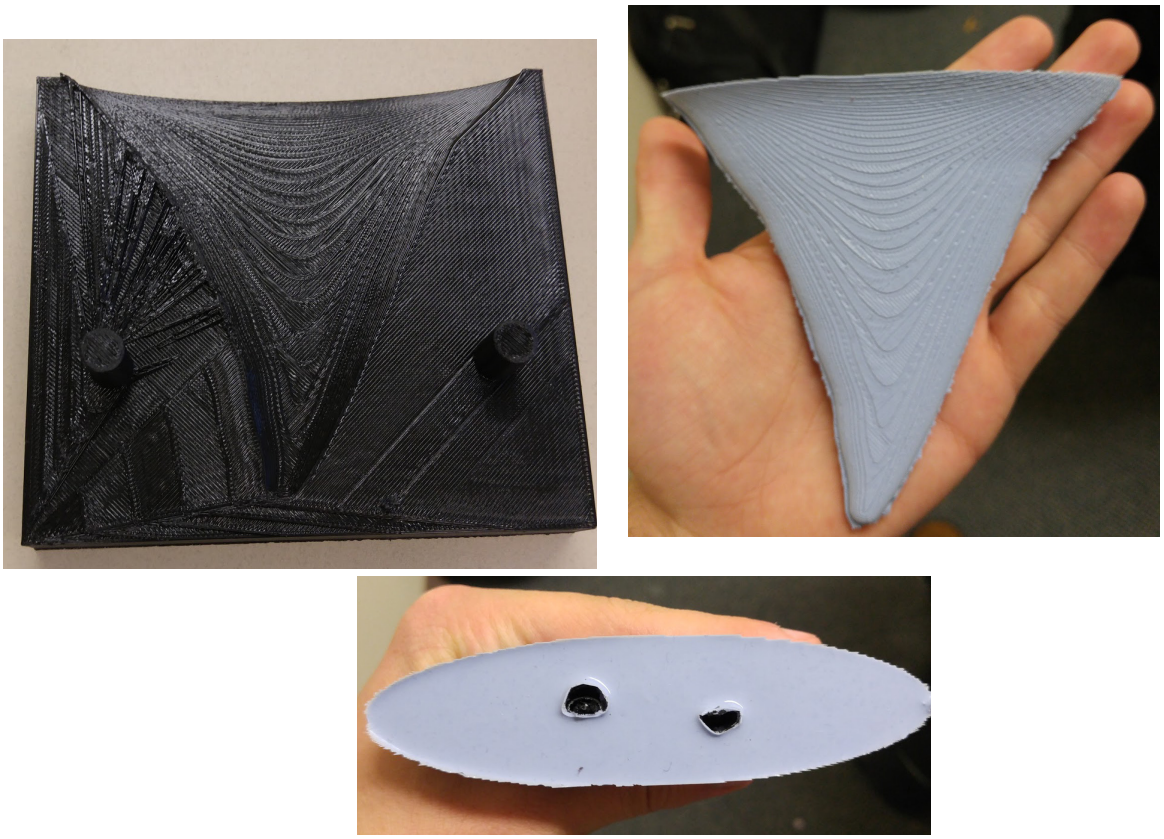

FIGURE 13: TWO CHANNEL FULL FIN MOLD AND OOMOO POSITIVE

To test it, a manual bike pump was attached to the inlet hole of one channel and pressurized air was pumped in. This prototype fin failed to actuate because the channels did not provide sufficient area for the length and thickness of the silicone.

Another small full fin was cast with the same foam and string concept, but one large channel was created with the intent of decreasing the amount of silicone that needed to be actuated. The channel followed the same shape as the fin, keeping a consistent edge size. The inextensible string was along one side, which meant the fin would theoretically only bend in one direction when filled air.

There was a minimal amount of actuation when this was tested because the silicone proved to be too thick. Cutting down the edges improved deflection slightly, but after some more testing the strings began to fall out of the silicone. They were unable to be completely embedded in the silicone during the curing because of the way it was laid against the foam. This method was determined to be unreliable and inexact in implementation, so other methods were pursued.

3.4.2 Half Fin - Oomoo

The next method used to create the fin drew inspiration from the manufacturing techniques used for the WPI Soft Robotic Fish.[41] Instead of making one mold for one fin, the fin would be constructed of two symmetrical halves with an inextensible layer between them. Rather than embedding polystyrene or other materials for the channels fully in the silicone, the mold for half the fin utilized a panel that molded the channels directly into the silicone. This allowed for more precisely made channels and consistent models.

The new printed mold was slightly larger than the first, but maintained the shape and proportions of the first small scale fin, which had been modeled extensively in SolidWorks. The set of channels was designed with one main channel running from the fin root toward the tip of the fin. Four perpendicular channels were spaced equally across approximately one third of the fin. This way the outer two thirds of the fin remained passive, allowing for more natural motion. Additionally, this passive tip was intended to create beneficial vortices, providing greater thrust.[42,43] The channels were half cylinder shaped with a constant radius. The widths of the channels across the fin varied in an attempt to keep the distances to the leading and trailing edges the same.

An inextensible layer was created separately by laying a section of tulle mesh on a flat surface and pouring silicone over it. The mesh allowed the inextensible layer to bend and twist, but not stretch in any direction. Once the silicone half fin was set, the two parts were bonded together with more silicone. A small opening to the main channel allowed the connection to the bike pump.

The first test was promising, however, very quickly the bond around the channels started to fail. This resulted in essentially one large channel, but there was still some actuation in one direction which indicated that the inextensible layer was functioning properly. Attempts to cut open the fin and fix the bond around the channels with high strength adhesive failed, but did prove that super glue does not adhere well to silicone.

[41] (Marchese, Onal, & Rus, 2014)

[42] (Liu, et al., 2015)

[43] (Moored, Smith, Hester, Chang, & Bart-Smith)

3.4.3 Half Fin - Dragon Skin

Once the Oomoo had been used up, the decision was made to switch to Dragon Skin 10 for its increased compressibility, flexibility and elasticity. Dragon Skin 10 has a tensile strength of 475 psi, over twice that of Oomoo, and 1000% elongation at break.[44] The same half mold was cast once more with the new silicone. Using the old inextensible layer did not work because Oomoo does not bond to Dragon Skin. A new inextensible layer was created the same way as before, but with the Dragon Skin, and the two parts were bonded together.

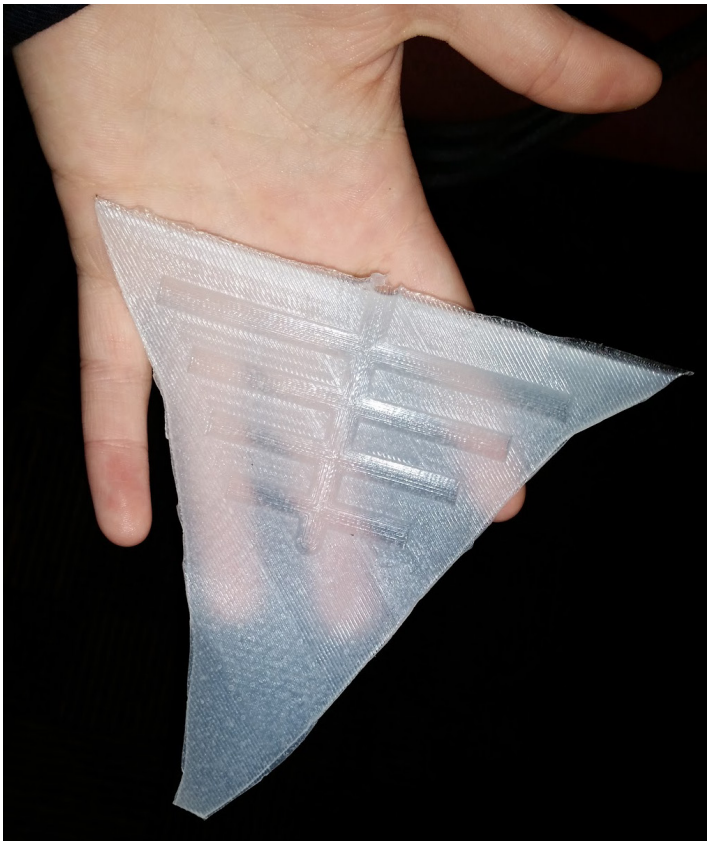

FIGURE 14: DRAGON SKIN UPPER FIN SECTION

During the bonding process, some of the channels filled in with the extra silicone, but there was still significant performance improvement using the Dragon Skin over the Oomoo. The material properties of the Dragon Skin allowed for more deflection from the fin root to tip. Because of the

[44] (Dragon Skin Series, 2015)

increased compressibility and elasticity, the fin was able to bend much more easily. Once again, after repeated testing the bonding between the channel walls and the inextensible layer started to weaken and eventually failed, separating the layers

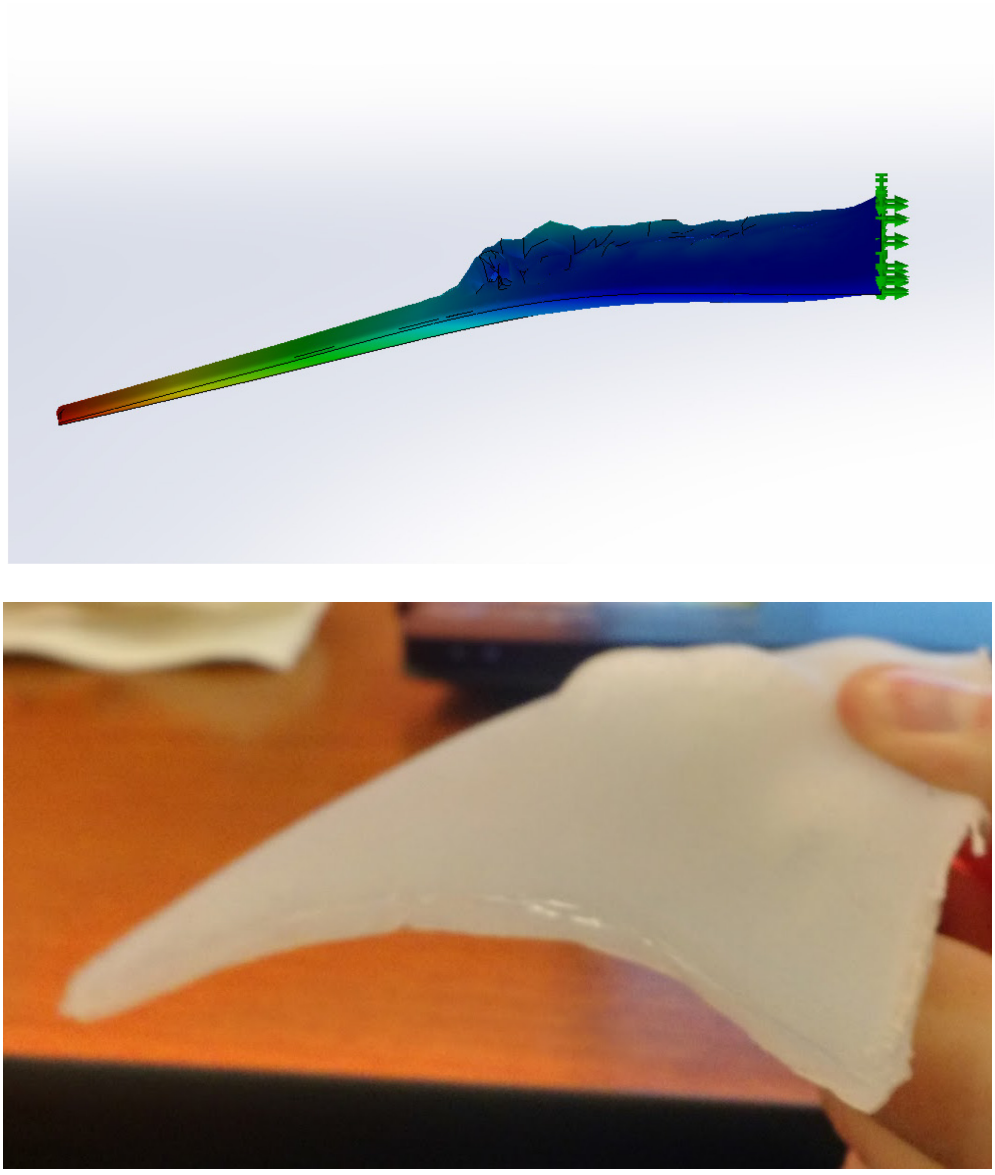

FIGURE 15: COMPARISON OF SOLIDWORKS SIMULATION WITH ACTUAL RESULTS

DRAGON SKIN HALF-FIN ITERATION 1

A new design was simulated in SolidWorks for the channel configuration of the same fin. A simple static simulation was conducted. The data sheet for the DragonSkin did not include all of the material properties required, so certain aspects needed to be derived. To complete a full half wing and

allow it to actuate, a very thin layer was added to close the channels. This layer had the material properties of Delrin acetal plastic, which is flexible but inelastic. The thick end of the fin was fixed and a pressure of 50 psi was added uniformly to the inner surfaces of the channels and areas of the inextensible layer that were covering the channels.

The semi-cylindrical channels were replaced with rectangular channels of varying depths such that their distances from the top of the fin were each the same. They were also much thinner and closer together. The simulations showed that this allowed more actuation with less bulging because the forces were more equally distributed and there was less material per channel to deform.

To try to avoid issues with the bonding failing between the fin and the inextensible layer, the silicone was poured onto the mesh and the fin was placed immediately on top of it. The intention was that the new silicone would bond well to the fin rather than depending on a very small amount of silicone to bond two separate pieces. With this method, channel loss was significantly reduced; only the last, smallest channel filled in.

This prototype was the most successful of the small scale tests with almost 90 degrees of actuation. There were a few places where the fin expanded perpendicular to the desired direction, with bulges where the material was thinner, which shows the consistency needs to be increased in future prototypes. With this improvement, this design was chosen for the final design.

While the 90 degrees of actuation was promising for the project, this was a result that deviated a significant from the SolidWorks simulation (Figure 3.4.3.3). This was most likely due to a more complex model than the previous fin and over-simplistic choice of simulation. In addition, the derived material properties for the DragonSkin represent a potential source for error. The confluence of factors likely resulted in the inaccurate simulation. Given the unreliability, the decision was made to discontinue simulating the models.

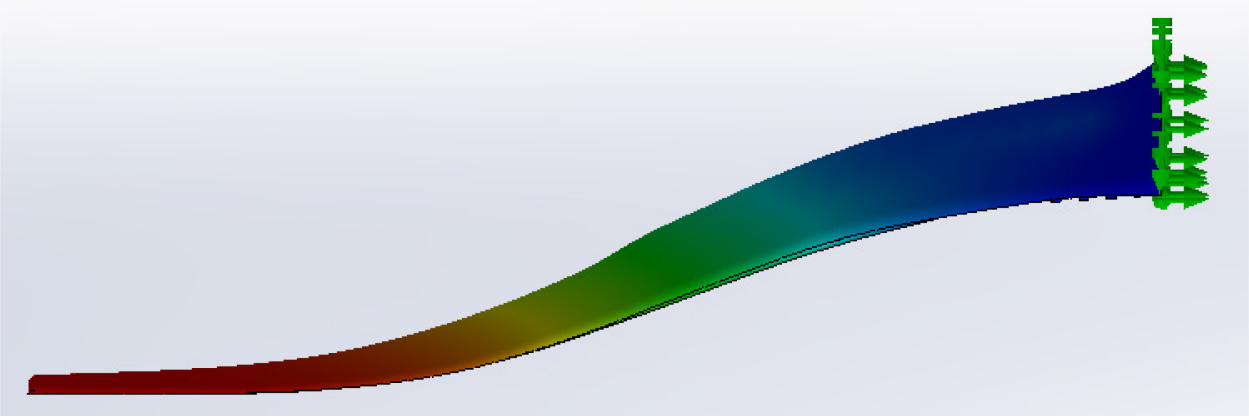

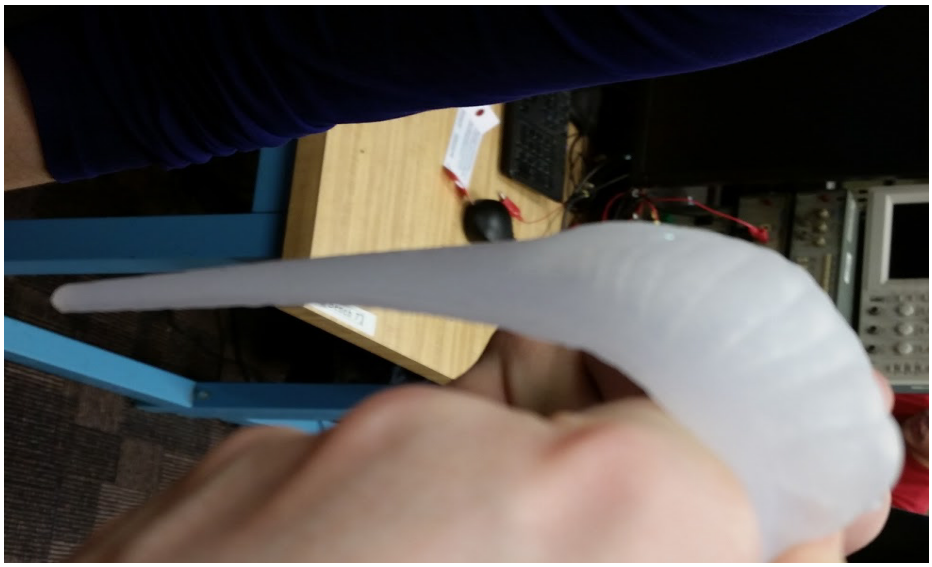

FIGURE 16: COMPARISON OF SOLIDWORKS SIMULATION WITH ACTUAL RESULTS

DRAGON SKIN HALF-FIN ITERATION 2

3.5 Fin Manufacturing Process

Due to limitations on rapid prototype molding, namely the build area of available 3D printers (approximately 10in x 6in with the Makerbot 2), it was not an appropriate production method for larger fins. Therefore, in order to create an 18in fin, a new production method had to be devised. In order to save on materials costs for testing iterations, before going directly to full scale from the small scale, it was decided to develop production methods with a medium scale fin.

In order to make a negative mold of an object, a positive is required. A small test was done with the high density foam, previously used to create channels, to see how difficult it would be to carve a fin

positive. Two pieces of foam were glued together to create a cube. From this point, using knives and rasps, a rough 6in foam fin was shaped by hand.

Once the positive was created, plaster was mixed as the mold material. Plaster is inexpensive, cures quickly and is a common material for making reusable molds. As proof of concept, the foam fin was suspended in a paper cup and the plaster was poured around it. Once set, the plaster block was cut in half to remove the fin.

FIGURE 17: SMALL SCALE PLASTER TEST

This process demonstrated that plaster could be used for a mold for a larger scale design. There were, however, a few things that needed to be improved. For instance, cutting the mold introduced potential for failure, as the plaster was prone to crumbling. To avoid cutting, the decision was made that the molds would be created for one half of the fin at a time, similar to the methodology employed for the small scale mold. Another place for improvement was the interface between the foam and the plaster. The foam was slightly pitted and porous, creating an imperfect mold.

With this new knowledge, it was decided the medium scale fin would be more feasible as the final prototype. This was based on the manufacturing time expected with each fin pour, and the cost of volume of silicone needed for the project.

4.0 Mechanical System Design

4.1 Design Considerations

In order to ensure the fin could be actuated, a target operating depth was determined. Using the generalization that every 10 meters of ocean depth causes a pressure increase of approximately 1 atm, the hydraulic system was designed to operate at depths of up to 20 meters. This generalization assumes water is perfectly incompressible, which is a reasonable simplification at this depth. At 1000m depth, water compresses less than one percent.[45]

Furthermore, research showed that coastal rays live between 0 and 80 feet (0 and 24 meters), spending the majority of their life between 30 and 35 feet (9 to 10.5 meters). This reinforces the choice of target depth.[46] Most coral reefs are less than 150 feet (45 meters) deep, although some extend as deep at 400 feet (122 meters). The current design would require an internal pressure of over 13 atm to safely operate at the 400 ft depth. While this is possible with the correct equipment, limited project budget and time frame make this impractical[47].

4.2 Hydraulic System Layout

A hydraulic system utilizes fluidic pressure to create motion. The hydraulic system is divided into two major loops. The high pressure side feeds from the pump outlet into each valve. From there, the valve can be opened to allow the working fluid under high pressure to enter the fin channel. When the valve closes, the fluid flows out of the fin into the low pressure line. The low pressure line feeds to the pump and the process is repeated.

[45] (Pressure at Depth, n.d.)

[46] (Manta Ray Advocates, 2016)

[47] (Basic Facts about Coral Reefs, 2015)

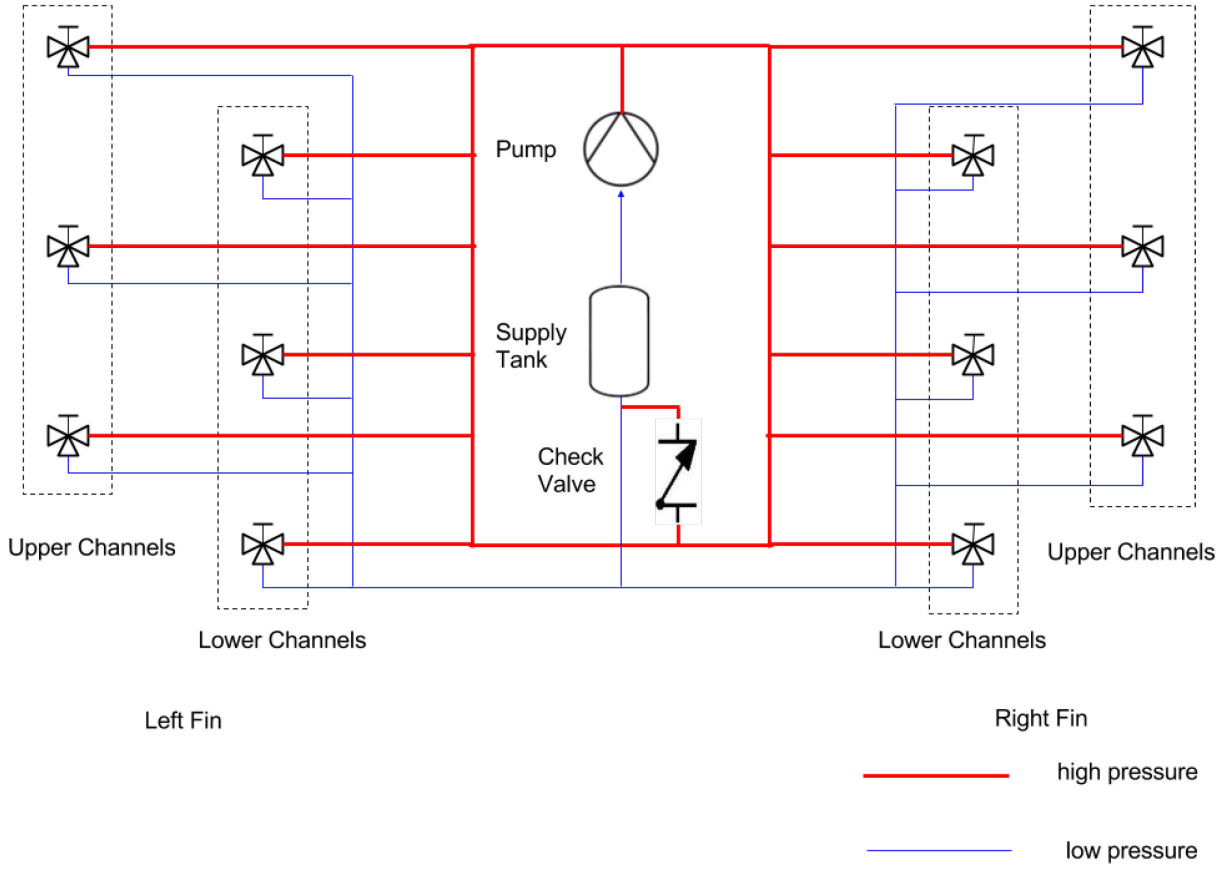

FIGURE 18: PLUMBING LAYOUT

4.3 Working Fluid

A hydraulic system requires a working fluid, or any fluid that is contained in the system. This fluid is pressurized, which is translated to mechanical energy through an actuator. The requirements for an ideal working fluid are that the fluid be incompressible, non-combustible, easily contained and with a constant viscosity. An additional consideration for this project was potential environmental impact. This leaves two common choices for working fluids; water and vegetable oil.[48] Water was chosen for this prototype in order to ensure ease of cleanup and availability of parts. Potential risks associated with

[48] (Garrett, 1998)

water as a working fluid include increased cavitation risk and narrower range of operating temperature.[49,50]

4.4 Pump

The pump is what creates pressure in a fluidic system. The pump for this project needed to deliver enough pressure for the robot to operate at the target depth, and be rated for usage with the working fluid. By choosing water, there was no need for a specialty pump, reducing both the price and lead time. The initial choice was a Flojet Demand Pump 1.6 GPM 12V DC 60 psi (FJC-PMP-D3131H5011A).

FIGURE 19: FLOJET PUMP [51]

The deciding factor in purchasing the pump was how much pressure it could provide. The Flojet pump 60 psi (4.1 atm) allowed for a significant safety margin. Running the pump at maximum pressure constantly can cause early wearing of parts and seals. This model can also run dry for short periods, ensuring the pump will not be damaged by a system leak. Electrical power draw is an important factor for an AUV, limiting choices of pumps further. The initial pump chosen requires 12V DC and draws 7A.

As the largest source of power draw in the project, the pump was a topic of continued research. Clark Solutions in Hudson, MA offered an educational discount on their MG200 gear pump, allowing greater pressure with less overall energy consumption. The MG200 provides up to 290 psi (20 atm) of

[49] (Water Hydraulics: Benefits and Limitations, 2015)

[50] (Is water hydraulics in your future?, 2015)

[51] (Flojet Pump [Digital Image], n.d.)

pressure while requiring 12V DC and drawing 3.4A peak.[52] This resulted in about half the power draw of the Flojet pump, while also being a significantly smaller, lighter, and quieter pump.

FIGURE 20: MG200 GEAR PUMP[53]

4.5 Valves

In order to control the pressurization and depressurization of the fin channels, controllable valves are necessary. The options were solenoid valves and motorized valves. Solenoid valves remain in a default state, either open or closed, and require a continuous energy draw to switch and hold the non-default state. Motorized valves require an energy draw to open or close, but can remain in that state with no draw. Solenoid valves are generally smaller and respond more quickly than motorized valves. The desired characteristics of the valve included a low current draw, rated for 60+ psi, and the ability to run off 12V DC. For this system design, a three way valve is required, further reducing valve options. The initial choice was the Misol 3 way motorized ball valve (DN15) due to its low price, availability, 800mA current draw, and ability to fit all other requirements.

[52] (Clark Solutions Gear Pump, 2014)

[53] (MG200 Gear Pump [Digital Image], n.d.)

FIGURE 21: 3-WAY VALVE [54]

Once one of these valves was acquired, it became clear a replacement would be necessary. While some small scale tests proved that the valve worked in the desired fashion, it was too large and heavy when considering twelve valves were needed. The time to switch the direction of the valve also introduced a delay between the desired change and the actual change. The results of these tests lead to the decision to acquire solenoid valves.

The valves used were the drip irrigation 3 way 12V solenoid valve from Ningbo Yaofeng Hydraulic Electrics Company. They are rated for a range of 9 to 150 psi and use 290 mA while holding.[55]

FIGURE 22: SOLENOID VALVE[56]

[54] (3-Way Mechanical Valve [Digital Image], n.d.)

[55] (Solenoid Irrigation 3-Way Valve, n.d.)

[56] (Solenoid Irrigation Valve [Digital Image], n.d.)

5.0 Electrical System Design

The electrical components of the robot depend heavily on requirements set by the other systems; motor voltage, current draw, sensors necessary for an intelligent control system, and size and weight restrictions all factor into the selection of parts. The electrical system collects data with sensors and outputs the power that drives the other systems. It allows the microcontroller to exert control on the rest of the robot, so it can be roughly equated to the robot's nervous system.

5.1 Microcontroller

The microcontroller is the brain of the robot, taking in data, performing computations, and controlling the actuators. There were several criteria important to choosing a microcontroller, such as digital I/O, available communication protocols, reliability and support. The ARM Cortex-M4 microprocessor was a favorable solution. The Cortex-M series is known for optimization of low cost, high performance, and low power. The M4F specifically is a 32-bit processor with a floating point unit (FPU).[57] This is helpful for the calculations required in dealing with various sensors.

Once the microprocessor was chosen, the microcontroller had to be picked. The top choices were the MSP432, STM32 L4 and AVR UC3 C-Series. The MSP432 was the final decision based on the features, including a 24-channel 14-bit analog to digital converter (ADC), 6 timers, UART, I2C and SPI communication interfaces, and a JTAG interface for debugging. For prototyping, the MSP432 is conveniently available in a development board, which features breakout pins, LEDs, switches, and available BoosterPacks for further functionality.[58]

[57] (Cortex-M Series, 2015)

[58] (TI LaunchPad, 2015)

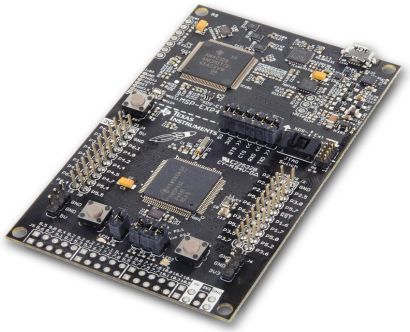

FIGURE 23: MSP-EXP432P401R (MSP432 LAUNCHPAD) [59]

5.2 Sensors

Sensors are the eyes and ears of the robot, providing input for the microcontroller. The sensors are split up into two categories: essential and payload. Essential sensors are used for determining orientation, depth, and other important information about the robot's state. Payload sensors are optional, used for data collection of the environment or other mission specific information. For this prototype, there are no payload sensors, but in the future they could be integrated with reasonable ease.

Below is the decision matrix for selecting the essential pressure sensor.

[59] (TI LaunchPad, 2015)

	Weight	Barometric Pressure Sensor	Submersible Pressure Transducer	MEMS Pressure Sensor
Resolution	2	2	1	1
Range	2	-1	1	2
Power Requirements	2	1	-1	1
Size	1	2	0	2
Cost	1	2	1	1
Unweighted Totals		6	2	**7**
Weighted Totals		8	3	**11**

FIGURE 24: TABLE 5.3.1: PRESSURE SENSOR CHARACTERISTICS

5.2.1 Inertial Measurement Unit

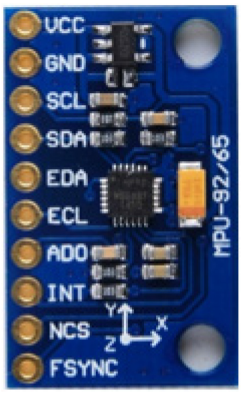

FIGURE 25: MPU-9250[60]

[60] (IMU [Digital Image], n.d.)

The first essential sensor board is the inertial measurement unit (IMU). This is a chip common for consumer electronics equipment, such as smartphones and wearable sensors, due to motion processing and MotionFusion algorithms.[61] The MPU-9150 was originally chosen for its 9-axis measurement from a 3-axis accelerometer, gyroscope and magnetometer. A breakout board was available from SparkFun with standard header pins for an easy interface. This chip was later replaced with the MPU-9250 - a newer model of the now-deprecated MPU-9150.

This board communicates with the MSP432 via I^2C. The MSP432 sends initial configuration information on powerup. Afterwards, certain registers on the board contain the continuously updated information for each axis of each sensor. The MSP432 then only has to send a request detailing the appropriate register, specified in the datasheet, and wait to receive the information which can be stored and used for processing. These values provide information about orientation that can applied to the control system.

5.2.2 Pressure Sensor

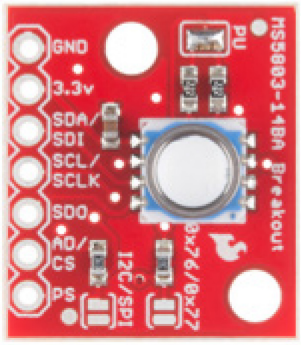

FIGURE 26: MS5803-14BA PRESSURE SENSOR[62]

The second essential sensor is the pressure sensor that monitors the robot's depth. The MS5803-14BA was selected due to its wide range, high precision, and availability on a breakout board from SparkFun for ease of use. This sensor is instrumental in giving the robot information about its position and developing failsafe systems.

[61] (IMU [Digital Image], n.d.)

[62] (Pressure Sensor [Digital Image], n.d.)

There are two communication protocols available with this board: I^2C and SPI. While SPI can transfer data at a higher rate, it requires more pins than I^2C. For this application, high speed sensor updates are not required. I^2C was chosen both for these reasons and to match the IMU. The way I^2C works, there can be one master with several slaves on the same bus. The MSP432 functions as the master and can continuously switch between the two sensors on the I^2C bus to update the information being processed.

An advantage of getting this sensor on the breakout board is the inclusion of an ADC. The MSP432 can send a request to the sensor board to convert the most recent value, wait a short time for the conversion to happen, then receive the updated sensor value. The result comes in a integer that can be converted into the pressure in millibar. The calculations require several factory calibrated values that are stored in the PROM of the chip. These constants are specific to each sensor and are easily retrieved by reading specific registers.

5.3 Power Systems

5.3.1 Batteries

The robot has two major systems requiring power. The first system is the propulsion, requiring a 12V battery, with significant current draw. This draws power only when the robot is pressurizing the hydraulic system or flapping.The second system, which consists of the microcontroller and sensors, requires 5V. The battery needed to be energy dense, rechargeable, stable long term, non-combustible, and environmentally friendly.[63] With these criteria, two types of batteries were considered for selection: lithium polymer (LiPo) and lithium iron phosphate (LiFePo4).

LiPo batteries were considered for their high energy density and commercial availability. LiPo batteries are commonly used and readily available for purchase.This eliminated any wait time on a custom order or risk of backordering. LiPo batteries are the lightest lithium battery, while still maintaining a high energy density, ensuring no unnecessary weight is added to the system. These batteries have a long life, are environmentally friendly, and are much safer than traditional lead-acid batteries. LiPo batteries are not perfectly charge stable, potentially exposing sensitive equipment to

[63] (Battery Selection, 2015)

voltage fluctuations. The pump and valve system is capable of withstanding small disturbances, however the sensors and microcontrollers could be susceptible to damage.[64]

LiFePo4 batteries, a type of lithium ion battery, were a promising option due to their increased performance when compared to other lithium polymer batteries. Being the safest lithium battery, they does not pose a risk to safety or the environment, and maintain the highest energy density of all lithium batteries to date. Additionally, LiFePo4 batteries have a minimum life span of 3 years from production date.[65,66]

FIGURE 27: LIFEPO4 BATTERY[67]

When actually purchasing the batteries, a small, light 12V LiFePo4 battery was found, with an included charging circuit, for a relatively low price. At 1.76lb and almost 50 in^3, this battery can fit easily in the hull without excessively disturbing the weight distribution.

At this point, rather than purchase a separate battery for the electronics, it was discovered that a voltage regulator would introduce significant price savings without significant energy loss. The LT1085

[64] (Battery Types, 2015)

[65] (Lithium Battery Overview, 2015)

[66] (Battery Types, 2015)

[67] (BatteryTender [Digital Image], n.d.)

voltage regulator is capable of shifting 12V to a stable 5V, with the implementation of some capacitors for stability. It is a relatively efficient chip that can handle 3A, which is enough current for all of the electronics. The other benefit of the voltage regulator is that the 5V output remains stable, preventing damage to the electronics from fluctuations.

5.3.2 Motor Drivers

In order to control the valves while providing the amount of power needed to switch and hold valve states, several L2930 H-Bridge motor drivers are used. This H-Bridge integrated chip takes an input signal from the microcontroller and adjusts the voltage of its output pins accordingly. The power output by the chip comes from battery power connected directly to the chip and is therefore not limited by the current ratings of the microcontroller. Each motor driver chip has four inputs and outputs, enough for four valves. However, for organizational purposes, four chips are used with three valves each so that every half-fin is attached its own motor driver.

The gear pump draws a steady 3.5A, which is more than the L2930s can provide, so a different motor driver chip had to be selected. The Pololu G2 High-Power Motor Driver 24v13 can handle 6.5-40V, well over what would be required for a safety margin for ripple voltage on the supply line. The continuous current capacity for the motor driver is rated at 13A, allowing for an inrush current of almost 400% of nominal current consumption.

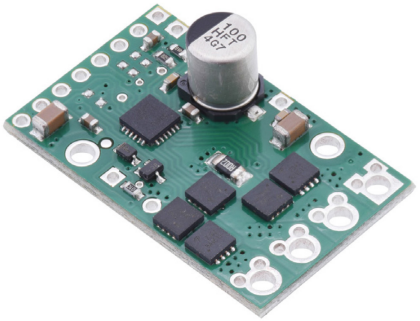

FIGURE 28: POLOLU G2 HIGH-POWER MOTOR DRIVER 24V13[68]

[68] (Pololu Motor Driver [Digital Image], n.d.)

6.0 Overall System Design

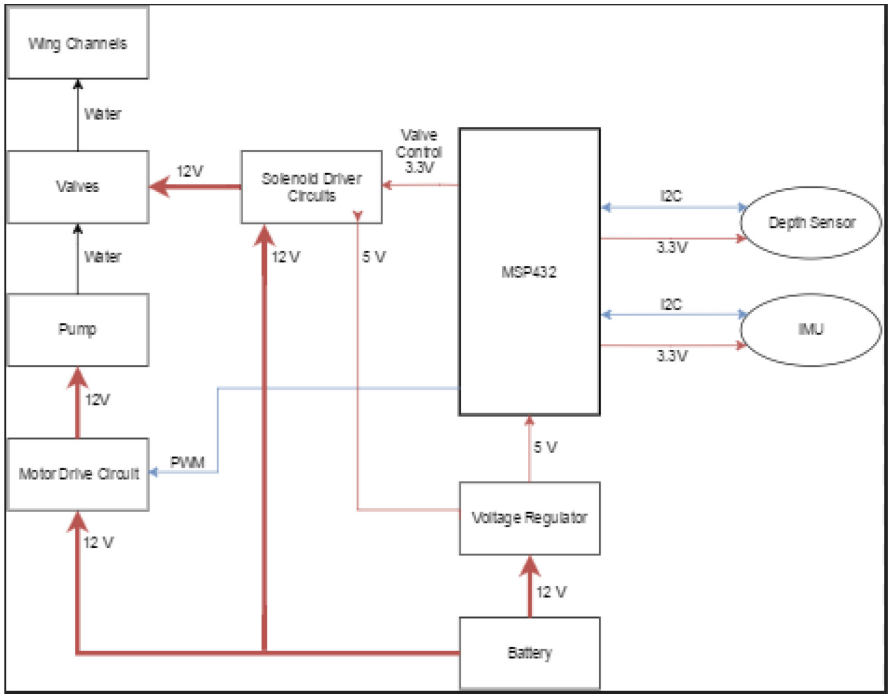

FIGURE 29: SYSTEM BLOCK DIAGRAM

6.1 Hull Design & Waterproofing

Ensuring the electrical and mechanical systems are protected from the water is vital for the survival of the prototype in an aquatic environment. As such, much consideration was put into the the robot's hull and waterproofing. All electronic components are housed within a smaller enclosure that is water resistant independent of the primary hull. The internal enclosure acts as a second defense should the primary hull leak. The plan was to buy a commercially available pressure vessel to ensure its success. This hull was planned to be rounded into a hydrodynamic shape by use of silicone. The primary hull had an access panel to allow for modifications and repairs to the internal components.

6.2 System Controls

Motion through the water is theoretically achieved by actuating each of the fin segments in sequence in order, creating sinusoidal motion. Each section is raised by both pressurizing the low channel set and draining the high channel set. Conversely, a section is lowered by pressurizing the high channel set, and draining the low channel set. The valves connect each partition to either high pressure when unpowered, or low pressure when the valve is powered, thereby filling, or draining its channel set.

By powering either the top or the bottom exclusively, and sequencing these top/bottom pairs from front to back, the fin may achieve sinusoidal motion.

In order to help achieve desirable movement, the robot's two sensors provide feedback about its pose in the water. The information from the IMU and pressure sensor is fed into the robot's microcontroller, the MSP432. A PID control prototype was developed to regulate the frequency of oscillation to move the robot around a horizontal plane.

6.3 Pinout Diagram

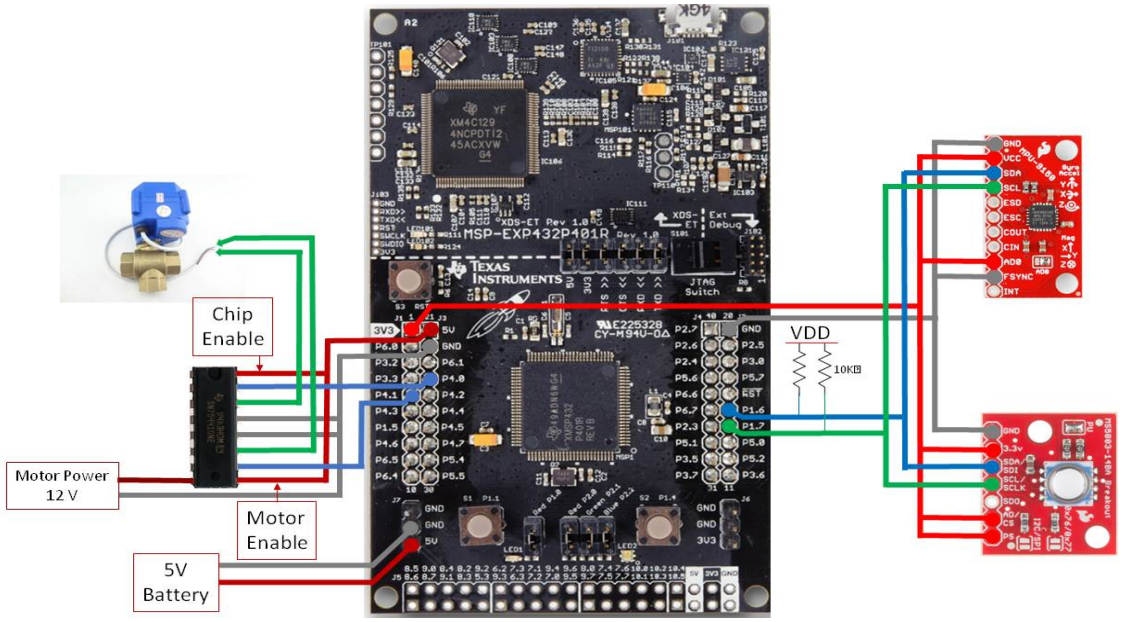

FIGURE 30: PINOUT DIAGRAM

Shown above is a pinout diagram of the MSP432 and peripheral electrical systems. The sensors on the right from top to bottom are the IMU and the pressure sensor. The SDA pins on both sensors are connected together and to the pin P1.6 on the MSP432. Likewise, the SCL pins are connected together and to P1.7. These form the I2C bus. SDA is the data line (blue), where information can be sent in either direction. For the purpose of this project, the MSP432 is the master, sending requests for information to the sensors. The sensors are the slaves, sending gathered data back to the MSP432 for processing. The SCL line (green) is for the clock. It is important that these are connected together and synchronized because bits are sent on clock cycles.

In order to control which sensor the MSP432 is communicating with, it needs to send the address of the slave with the start condition. Each sensor has an address as described in its datasheet.

For instance, the pressure sensor has the address 0b0111011n, where n is replaced with a 1 if the CSB pin is pulled high and 0 if the CSB pin is pulled low. This theoretically allows two of the same sensors to be placed on one bus. In this configuration, the pin is pulled high, so the address is 0b01110111. The IMU has a similar situation by pulling AD0 high, setting the LSB of the address to 1.

The PS pin on the pressure sensor is pulled high to select I2C mode, because it is also capable of communicating with SPI. The decision to communicate with this sensor using I2C was made to keep the communication protocol consistent with the IMU, which is only capable of I2C.

To the left of the MSP is the H-bridge motor driver circuit. Motor power (dark red) is provided by a 12V battery, and chip power (chip enable) is provided by the MSP (light red). Ground for the circuit (grey) is connected to both the MSP ground and ground of the battery. By providing a PWM signal from P4.0 and P4.1 (blue), the voltage level at the adjacent output pins (green) can be controlled. With no input signal, the corresponding output pin will be grounded, and with a 100% duty cycle (a high pin) input, the output will be motor power (12 V). By driving one input pin low and the other high, a voltage difference of 12 V in one direction is created across the valve's power cables. The direction can be switched by swapping which input pin is high and which is low. By this method, the valve can be driven in either direction at the command of the microcontroller. By mirroring the input, output, and ground pins across the H-bridge, and connecting them to different input pins, another valve, and the same ground rail (grey) respectively, a second valve can be driven through the same motor driver chip. In order for this to work, the top-left pin, which serves as the second half's motor enable, must be connected to the 5 V (light red) rail.

6.4 Design Limitations

Common silicone exists that can withstand up to 1200 psi (80 atm) allowing a depth of almost a half mile (800 meters), proving the feasibility of a deeper diving model.[69] It is worth noting this design is not feasible for extreme depth, as the average ocean depth is 2.3 miles (3700 meters) and would require over 370 atm of pressure to reach. The limitations on flexible enough materials make this a current impossibility.[70]

[69] (COHRlastic Silicone Rubber Products, 2015)

[70] (NOAA, 2015)

7.0 Projected Budget

In order to better organize the project, an estimated budget was established. The following figures are rounded up and account for shipping, taxes, and has anticipated extra required parts. Most of the needed tools and equipment were provided by WPI or team members' personal supplies. For this reason, tool costs were not included in the budget.

Material	Description	Units Used	Cost per Unit	Total Cost
Silicon for Molding	material for molding fins	1	$200.00	$200.00
Hull Casing	pressure housing for components	1	$500.00	$500.00
Pump	pressurization of fluid for actuation	1	$120.00	$120.00
Valves	automated valves to control actuation	12	$25.00	$300.00
Reservoir Tank	tank to hold excess hydraulic fluid	1	$10.00	$10.00
PVC Piping	piping & fittings used for pressure system (ft)	20	$2.50	$50.00
Hydraulic Fluid	working fluid in our system	1	$20.00	$20.00
Large Battery	power for the pump and valves	1	$60.00	$60.00
Small Battery	power for the micro-controller	1	$20.00	$20.00
Large Motor Driver Circuit	system to power pump	1	$30.00	$30.00
Small Motor Driver Circuit	system to power 2 valves	6	$5.00	$30.00
Microcontroller	"the brain" of the robot	1	$25.00	$25.00
IMU	sensor for navigation in water	1	$30.00	$30.00

Pressure Sensor	**sensor for safe depth detection**	**1**	**$65.00**	**$65.00**
Other ECE Components	**misc parts needed for interfacing**	**1**	**$40.00**	**$40.00**

Project Total: $1,500.00

FIGURE 31: ESTIMATED BUDGET BREAKDOWN

8.0 Fabrication

8.1 Fin Fabrication

With the manufacturing process established through the iterations of smaller prototypes, full scale fabrication was started. Each iteration of the manufacturing process was further refined to improve the results and progress toward a functioning set of fins.

The full scale model used two foam positives, one of each half of a fin, to make plaster negative molds. One set of two, mirror imaged molds was capable of creating both of the full fins. Each 18in mold was cast directly into a wooden box so that it did not have to be cut or moved. The plaster was set as a reusable mold. Similar to the small scale, silicone was poured into the positive and channel inserts were pressed into the wet silicone. The full scale channel mold made the progression from a single set of channels to multiple independent sets.

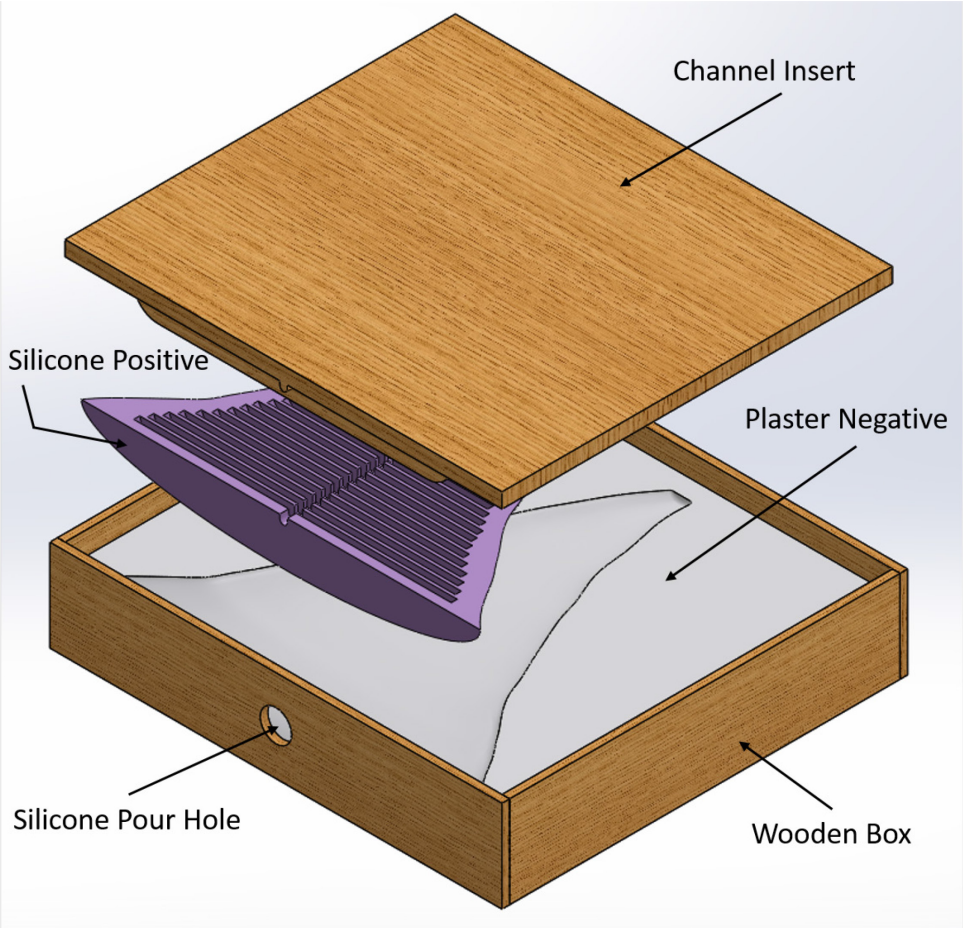

FIGURE 32: EXPLODED VIEW OF PLASTER MOLD

The advantage to using incremental scaling was the ability to test and make improvements while being more time and resource efficient. The downside was that each iteration added to the cumulative time commitment of labor not being applied directly to the final model.

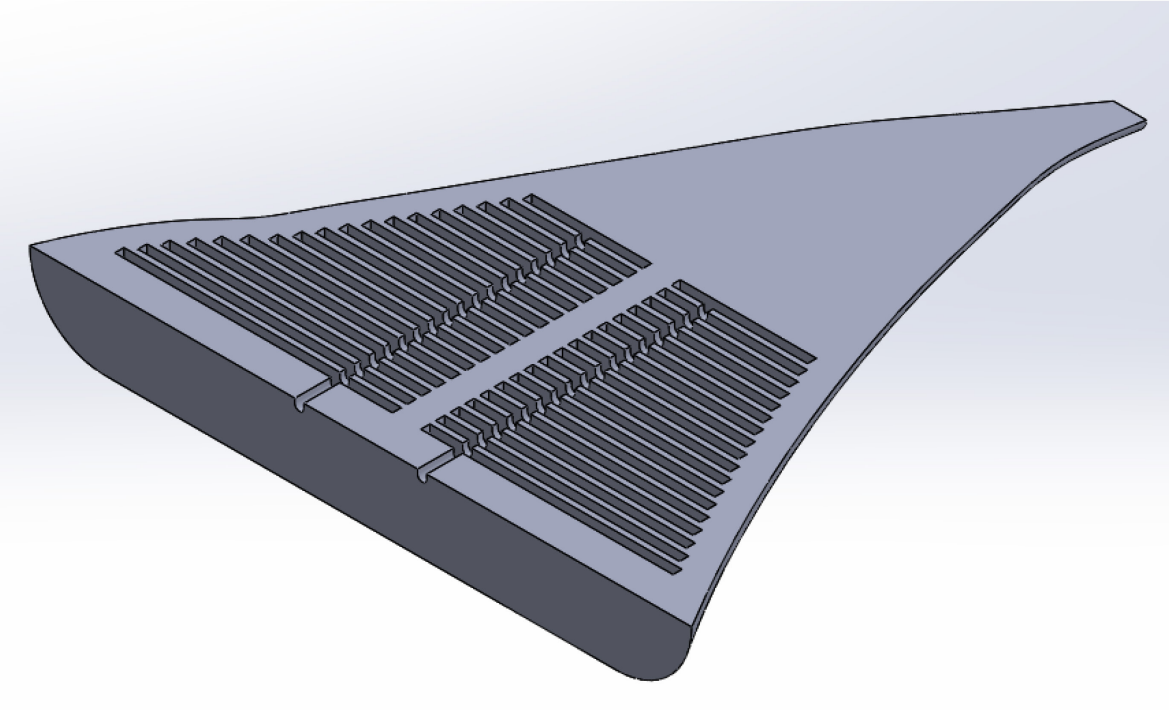

FIGURE 33: SOLIDWORKS MODEL OF HALF FIN

8.1.1 Final Fin - First Attempt

The first full scale attempt incorporated some changes and improvements from the small scale models. One change was the way the channels made. Where the small scale channel mold was created with a 3-D printer, the full scale channel insert was constructed on a panel made of wood that was set on top to close the box.

The next step was making a foam positive of the fin. For a precise recreation based on the SolidWorks model, the plan was to use WPI's ABB Robotic Arm. This robot is capable of using an endmill

attachment to carve materials, like foam, from multiple angles. This is where one of the larger obstacles was encountered. The ABB Robotic Arm can be operated either in a manual mode, or run from a program generated using ABB's RobotStudio software. Due to the complex nature of the fin shape, manual operation was unlikely to be successful. As such, the offline programming method was pursued. To do this, a digital workstation was set up in RobotStudio, which included a model of the robot that would be used for actual manufacturing. With this set up, a SolidWorks model of the midscale fin was imported into the work station. To facilitate easier modeling of the robot operation, slices were added to the fin model prior to importing it into RobotStudio. These slices were oriented across the fin, parallel to the root. The slices in the solid model generated distinct edges along both sides of them. This feature allowed the use of the AutoPath tool. AutoPath allows RobotStudio to detect an edge around a selected object, and generate a tool path along that edge. Using this method, the surface of the fin was traced. Once all of the tool paths were generated, the program was loaded to a USB drive, and transferred to the robot.

Before any actual cutting of foam was to be done, the program was tested on the robot. This was where some problems were encountered. The first problem noticed was that the robot's Joint 6, which corresponds to the rotational aspect of the robot's "wrist" joint, was turning excessively, slowing the actual movement of the robot. While this issue was a slight slowdown, it could be dealt with. The major issue arose when the robot moved along the second path. The robot began encountering a singularity that did not appear in the simulation. This caused Joint 4, which rotates what could be thought of as the robot's "forearm," about an axis through the link, to rotate all the way to its limit, which was then detected by the robot controller and stopped the entire program. Several attempts to fix this problem were made, including manually setting the configuration of the robot at each individual target point. Another technique attempted was to add intermediate target points along the path that was generating the singularity. This was done in an attempt to force the robot to maintain a preferred orientation. Both of these attempts were ultimately unsuccessful.

Since the singularity in the robot was encountered approximately half way across the width of the fin, it was agreed that not transiting the entire width with the robot might solve the problem. To accomplish this, another slice was made in the SolidWorks model. This time the slice was oriented along the length of the fin, from the root to the tip, and perpendicular to the previous slices. The final model with the slices is shown in Figure 8.1.1. This created additional edges to create paths on. At this point a path could be generated from the outer edge of the fin, across the top surface, to the midpoint of the

fin, and back to the outer edge with one continuous path. Pre-production testing verified that this method did solve the singularity problem, and the program was able to run all the way through.

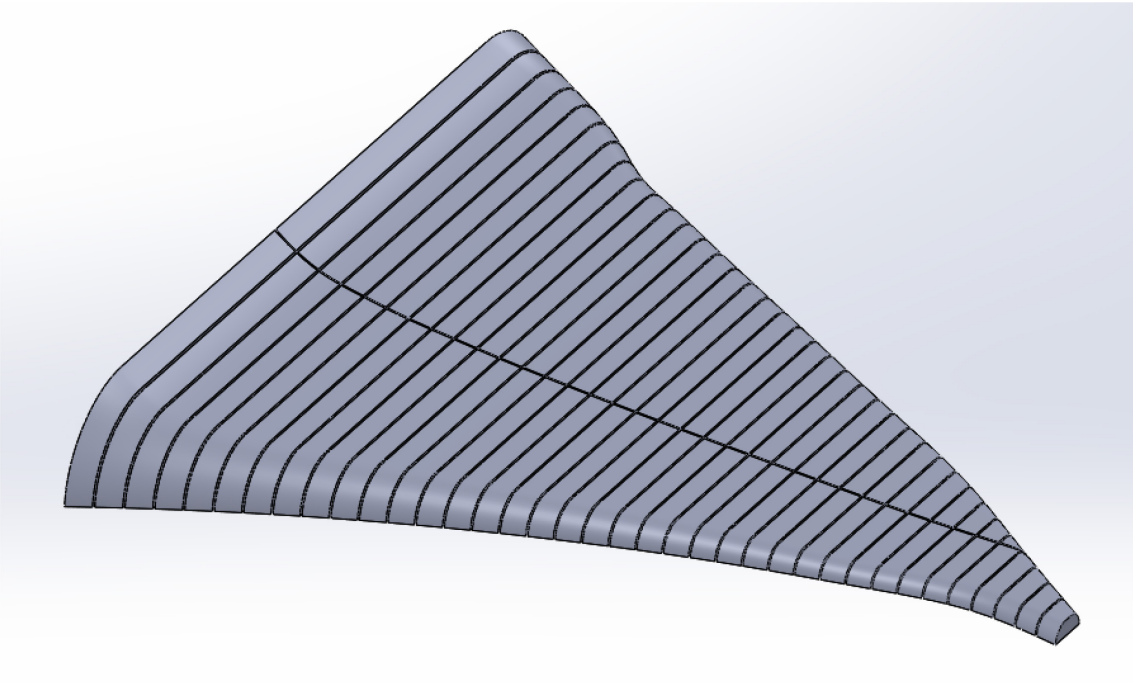

FIGURE 34: FIN MODEL WITH SLICES

The last task that needed to be accomplished before cutting the foam with the ABB robot was to build a platform for the offset height above the work station surface. This offset is required because the end mill used for the carving is attached to the robot via a 5” diameter bolting flange. This flange would hit the surface of the work station when attempting to carve the lower sections of the fin if there was not an offset applied to the work piece. To create the offset required, a platform was constructed. This was done using a spare section of MDF and some scraps of 2in x 4in wood. Nails were pushed through the bottom of the MDF to hold the foam block in place while it was being carved.

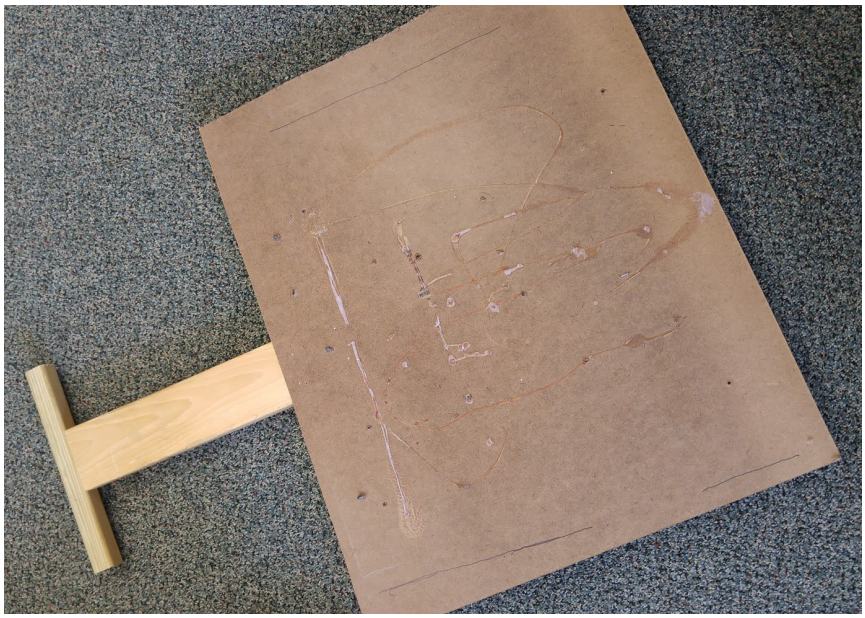

FIGURE 35: MOUNTING PLATFORM FOR FOAM

With the program working and the offset platform constructed, a first attempt at carving was made. However, it was soon discovered that additional preparation was needed before this process would work as planned. One major issue was that the end mill being used only had 1.5” of cutting length. This meant that any areas needing to have more than 1.5” of foam removed had to be reduced manually. Additionally, it was discovered that the speed setting on the robot was much too high for the cutting capability of the end mill. This was fixed by reducing the speed setting of the robot in RobotStudio.

With these issues resolved, carving was once again attempted. This time attempt was much more successful, and only a few incidents occurred where the DC motor powering the end mill was bogged down while cutting. This was overcome by manually pausing the program, letting the motor spool back up, and continuing the program. This attempt was cut short due to time constraints.

Eventually, in order to keep up with time constraints, the foam for the first fin model was hand carved using a hot wire foam cutter, a hacksaw and several methods of sanding. Next, a shallow box was constructed out of medium density fiberboard (MDF), which allowed a structure for the plaster pour. The first attempt at the plaster negative failed because the mixing process was too slow. This resulted in the plaster hardening in the bucket before it could all be added to the box. Once it was dry, the plaster also crumbled easily along the edges, which resulted in a delicate mold. In order to resolve this issue,

jointing compound was used for the second attempt. Jointing compound is a mix of plaster of paris and several other hardening agents, which results in a more homogenous mixture and consistent strength. Foam was inserted into the corners to reduce the amount of jointing compound required for the mold.

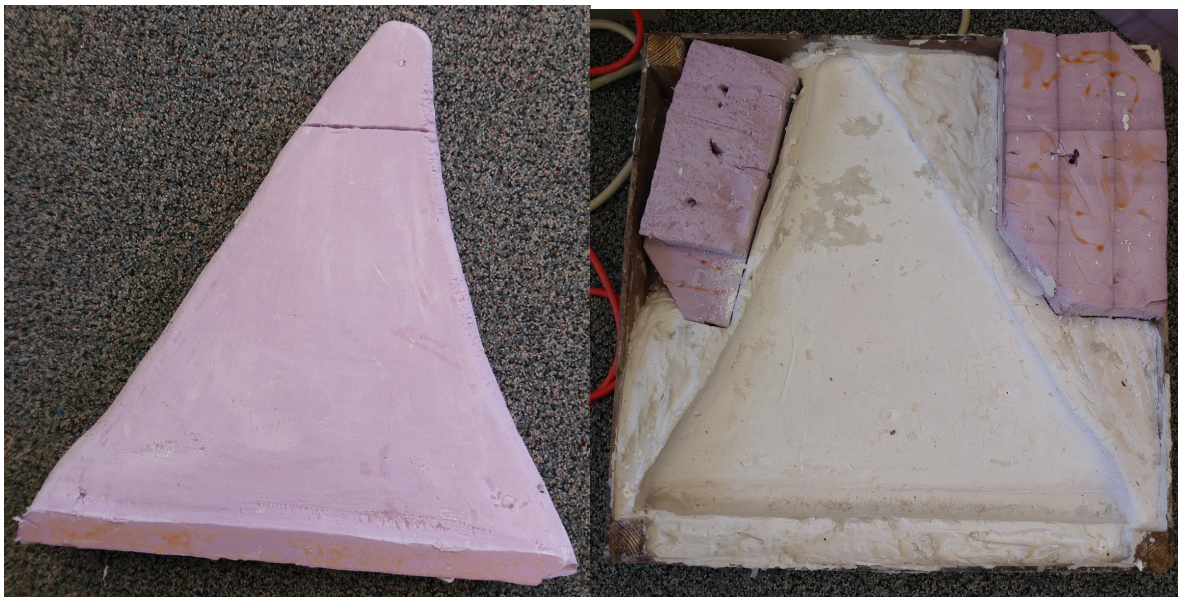

FIGURE 36: FOAM POSITIVE AND PLASTER NEGATIVE MOLD

To complete the mold, the channel inserts need to be created. In order to reduce cost and lead time, basswood was decided on for constructing the channel inserts. Using a layer of MDF, the basswood was layered on and cut to the channel dimensions as they had been defined in the SolidWorks model. This process involved sanding the basswood down to size and wood gluing the pieces onto sketches derived from the SolidWorks model for the channel geometry. This proved to be a tedious and inaccurate process. During gluing, many pieces slipped slightly, and cuts were found to be too rough to fit perfectly together. The channels were all less than three centimeters, much too small to work with by hand with any true accuracy.

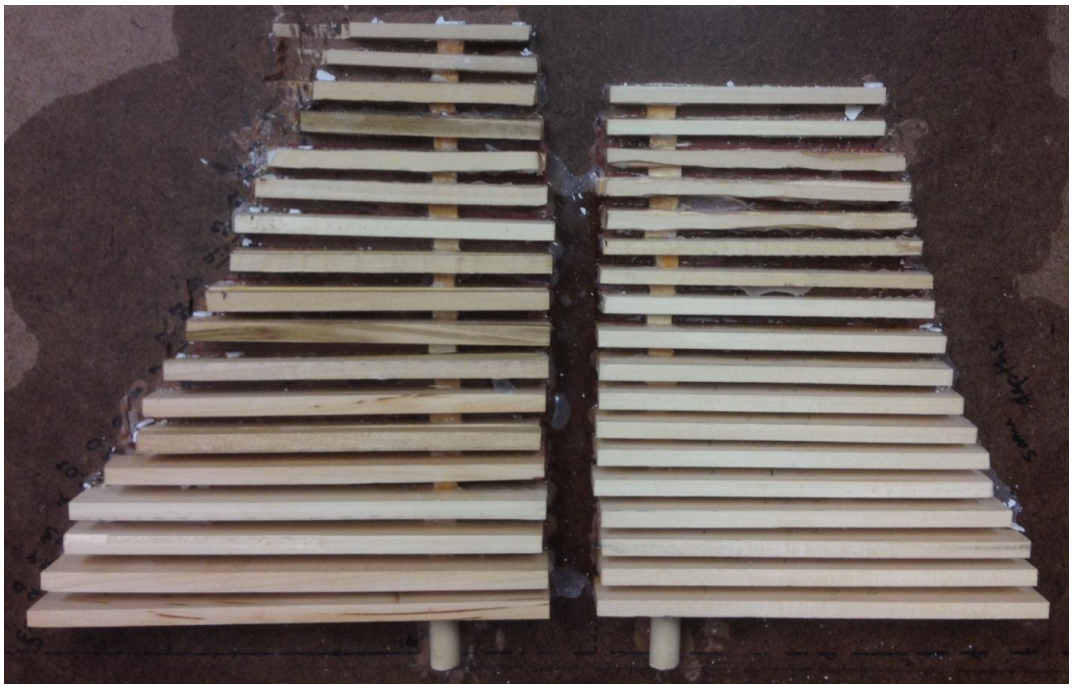

FIGURE 37: BASSWOOD CHANNEL INSERTS

With the requisite parts completed, the mold was ready for the silicone to be poured. The same silicone that was used in the small scale was used in the full scale, Dragonskin 10. There was concern with bubbles forming in the mixture and compromising the channel structure. To avoid this, an improvised degassing chamber was created using Space Bags and a shop vacuum. The silicone was poured and degassed according to plan, however, the channel inserts floated slightly while the silicone was curing, resulting in insufficient channel depth.

In order to mitigate loss, an attempt at an inextensible layer was made on this unusable fin. Delrin was used in the soft robotic fish project, but proved expensive and difficult to obtain. Instead, a high density plastic layer was used, as it was assumed to have similar properties. The process for bonding the inextensible layer to the fin was the same as the one used in the small scale prototype, and appeared to have worked well. This turned out to not be the case when the fin was subject to significant deformation and the high density plastic pulled out of the silicone.

On the second fin, holes were made in the high density plastic to allow the silicone to bond better. The layer was attached like the others, and once again pulled free under significant deformation of the fin. With neither solution producing acceptable results, other material options were explored.

8.1.2 Final Fin - Second Attempt

Applying the lessons learned from the first full sized attempt, accurate channels were created with a 3D printer. This had not been the first course of action because the full set of channels was too large for the build area of the printers that were available. After making the positive in SolidWorks using the existing fin model, it was split into three sections that could be printed individually. The three parts were glued into one panel using a two part epoxy.

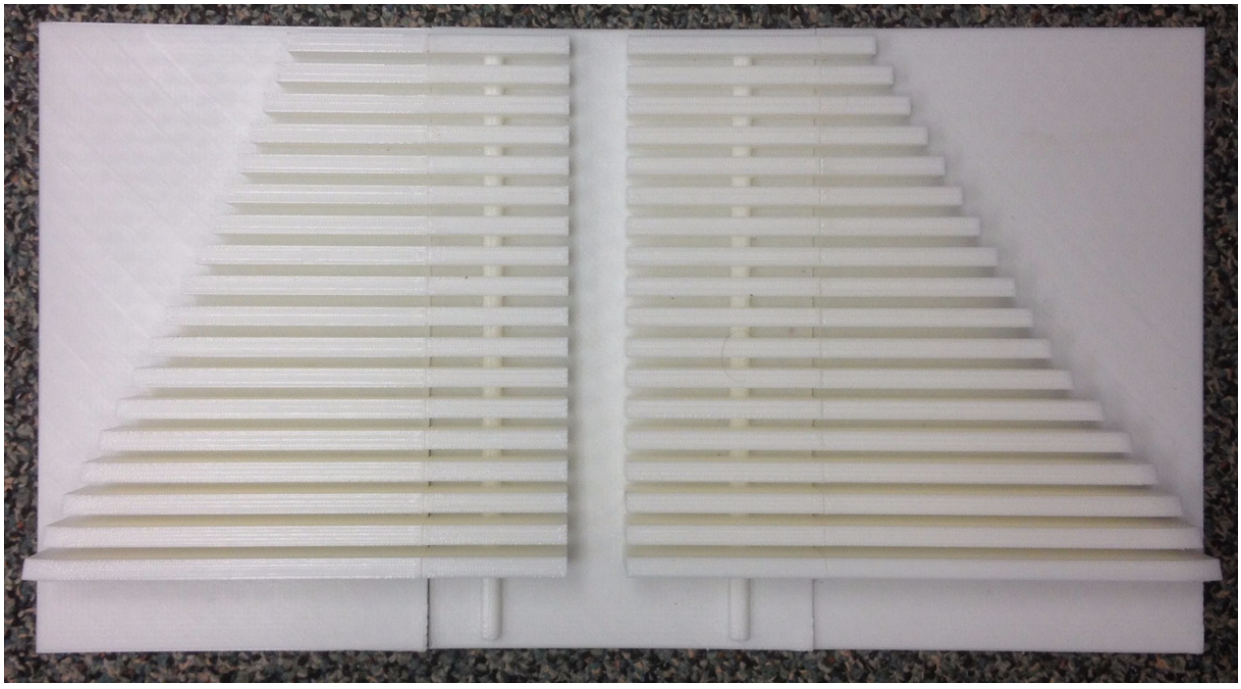

FIGURE 38: 3D PRINTED CHANNEL INSERTS

The process for pouring the silicone, setting the channels and degassing was the same, except the channel inserts stayed deep in the silicone mixture and remained in place. The mixture was degassed and left overnight. Difficulty was encountered separating the mold from the silicone. As a result, two of the three 3D printed channel inserts broke while being removed. It was also discovered that the silicone mixture never fully cured and remained quite sticky, causing some slight issues with fin. Given that the stickiness remained indefinitely, it was likely because of either an imbalance in the silicone parts ratio or insufficient mixing of the combination. In order to prevent this error from recurring, investment was made into better mixing equipment to assist in ensuring successful attempts in the future.

FIGURE 39: BROKEN CHANNEL INSERTS

Once again, to reduce waste, another test of the inextensible layer was conducted. Using the example set by the small scale test, a mesh was used for better bonding. Window screen fit all the requirements of an inextensible layer, so a new layer was made and the results were quite promising. Under significant deformation, the screen showed no sign of separation. With this result, the inextensible layer issue seemed to be resolved.

FIGURE 40: SUCCESSFUL INEXTENSIBLE LAYER

8.1.3 Final Fin - Third Attempt

After the frustration of the second attempt, the process was revised and a third pour was set up. In an attempt to be more efficient, two fin halves were planned to be poured simultaneously. The channel inserts needed to be 3D printed again, but, instead of being cemented together, the segments were attached to cardboard and taped in place to allow easier removal without the risk of the channel segments shifting while the silicone cured. Disposable cups were used to ensure a 1:1 ratio of silicone mixing parts, and the silicone mixture was stirred thoroughly in a second container before being poured. Once the silicone was poured, the channels were carefully inserted and the mold was inserted into a Space Bag for degassing. A shop vac was used to remove the air from the space bag, thus removing air from the silicone. In the process, the channel inserts were pressed into the silicone, and some silicone was vacuumed up.

Removing the channels on the cured fin was difficult once again. The 3D printed channels cracked, but were not badly damaged. The cracks were glued so the channels could be reused. Both fins were unusable, the first had considerable air trapped inside, creating bubbles, while the second fin's channels penetrated the outside of the fin, compromising the ability to hold fluid. It was determined

that the cause of this was the degassing procedure. For the first fin, it was likely the air was drawn to the top of the fin mold and was then trapped, leaving large hollow sections of the fin. The second fin appeared to have fared due the channel inserts being pushed too deep into the mold.

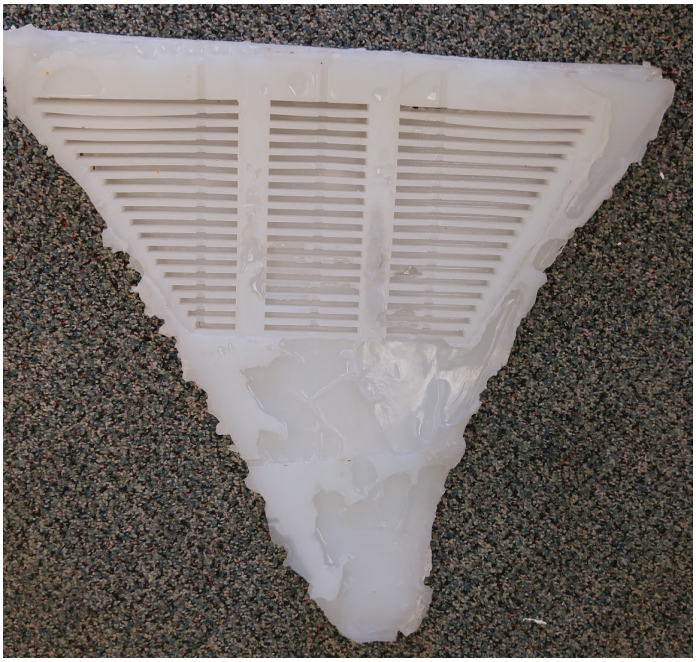

FIGURE 41: FAILED FIN - SILICONE BUBBLING

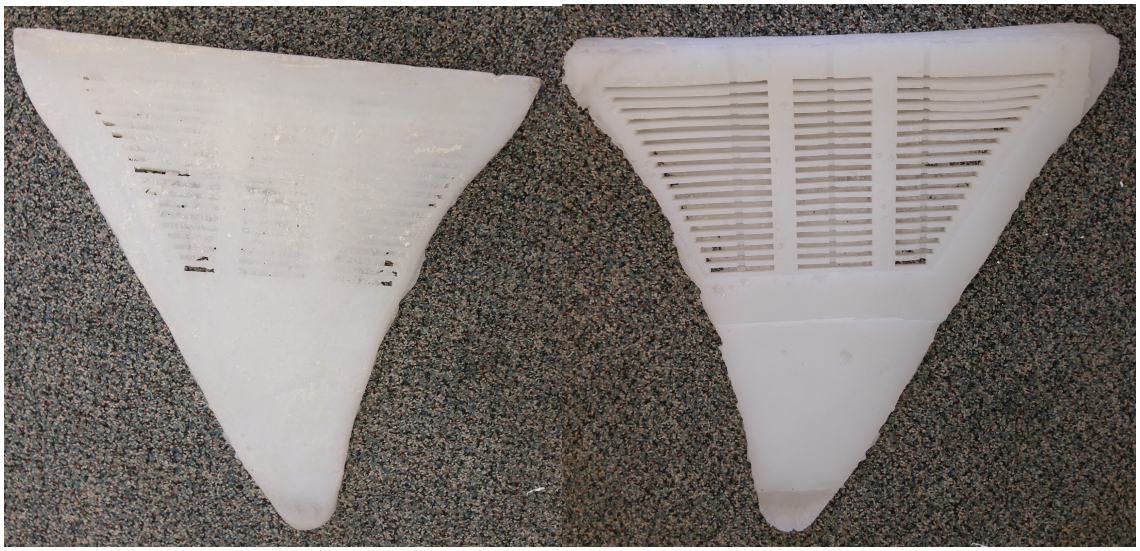

FIGURE 42: FAILED WING - SHALLOW CHANNELS

8.1.4 Final Fin - Fourth Attempt

Electing to avoid degassing on the final prototype, another pour was attempted. This time the channel inserts were held with tape and cardboard to allow disassembly for making the channel removal easier. The channel inserts were also supported along their top edge to prevent them from sinking too far into the silicone. By eliminating the degassing step, the resulting fin was properly formed and the channel inserts came out easily with their segmented design.

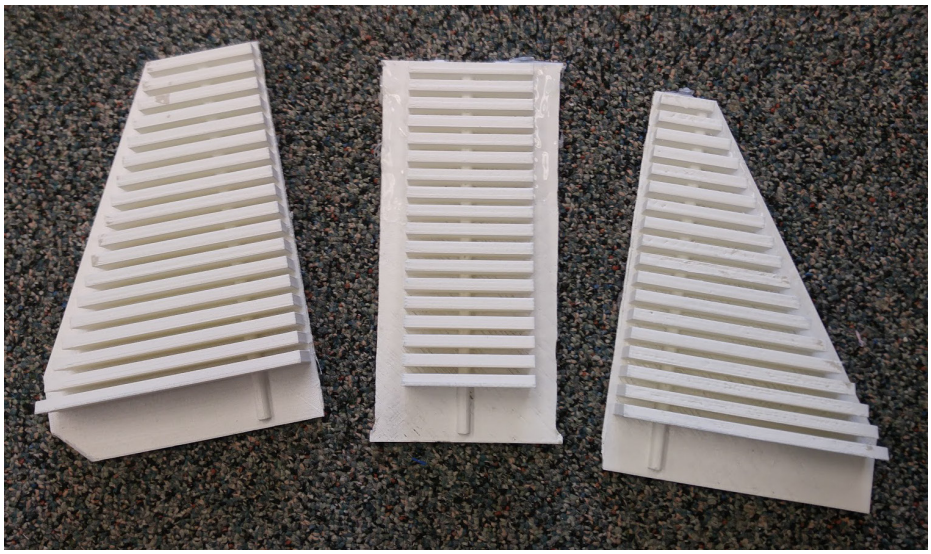

FIGURE 43: SEPARATED 3D PRINTED CHANNEL INSERTS

With positive results using window screen for an inextensible layer, the decision was made to continue with this technique. The inextensible layer was bonded to two of the four fin halves. Once these were cured, the two remaining fin halves were attached, creating two full fins.

8.2 Hull Fabrication

Upon further research, the cost of a premade pressure vessel was found to be prohibitive. Additionally, the prototype did not require much pressure resistance. Through reaching out to contacts, the suggestion was made to use fiberglass, due to the cost, short fabrication time, and reduced depth requirements.

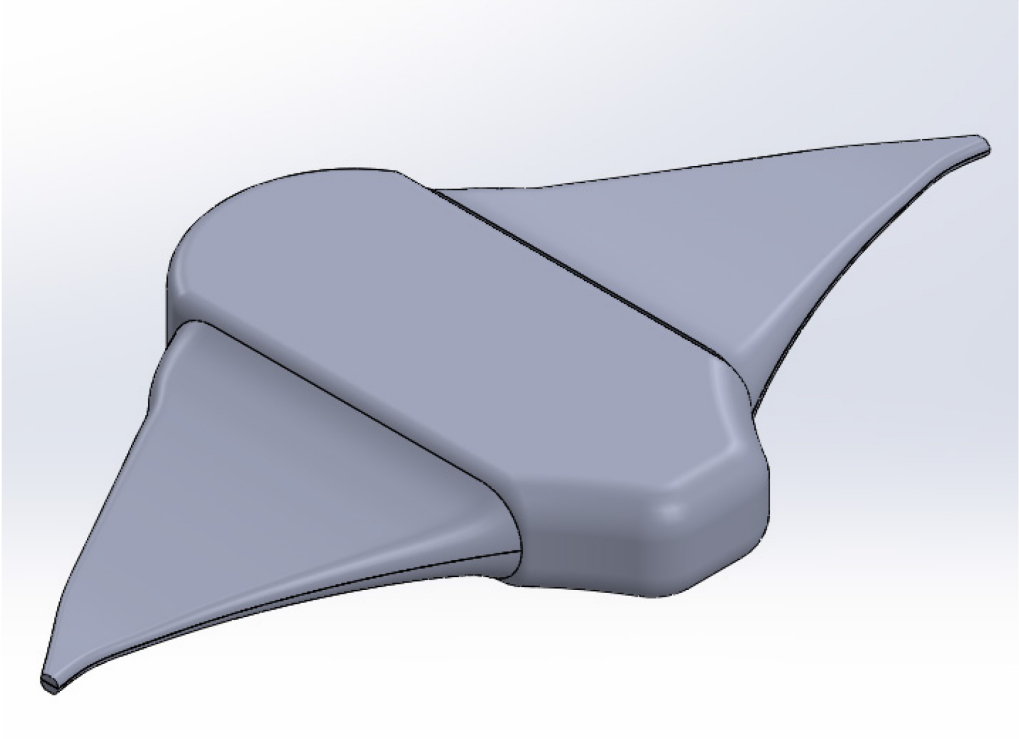

FIGURE 44: SOLIDWORKS MODEL OF MANTA RAY ROBOT'S FINS AND HULL

A SolidWorks model of the hull was created and put into an assembly with the full fins to confirm the proper dimensions and shape. Using this model for the hull, foam was cut to the shape needed and smoothed out. Similar to the fin, the hull uses foam blocks, cut to size, as a foundation for the structure. Due to the limited time with the ABB Robotic Arm, the foam was shaped by hand.

WPI's SAE Formula Car project team had also used hollow body fiber glassing, and warned of their failure to obtain the proper shape with it. Acetone in the fiberglass resin dissolves the foam as the fiberglass cured, leading to deformation of the structure. This was mitigated with a layer of paper mache to provide a barrier and additional support. The paper mache was wrapped with aluminum foil to further protect the foam from the resin. The fiberglass fabric was wound around the hardened structure, and then treated with the resin. Upon curing, the fiberglass hull proved to be solid, with minor integrity issues at the rounded edges. The foam survived the fiber glassing, and required an acetone bath to clean out the hull. Upon testing, the fiberglass hull showed significant leaking and required extensive patching. After multiple attempts to patch the hull with various forms of epoxy and caulk, the decision was made to direct efforts toward a new hull.

FIGURE 45: FIBERGLASS HULL ATTEMPT

The second iteration of the hull was created from acrylic. The acrylic was hand cut and chemically welded. Once bonded, the hull showed no sign of leaks. The next stage was to drill holes for the fin tubing. This was carefully done by incrementally increasing drill bit size. The tubes were threaded through these openings then silicone caulked in place. In order to ensure access to the internal components, a hatch was integrated to the top of the acrylic hull. This was accomplished by cutting the top piece of the hull in half and removing enough material to fit the hatch in place. The halves were then chemically welded together with an additional piece of acrylic on top. This ensured the halves were properly sealed.

FIGURE 46: ACRYLIC HULL AND HULL HATCH

8.3 Plumbing Assembly

The plumbing assembly started with a simple test of the pump, a Flojet diaphragm pump. A quick connector was used with flexible tubing able to withstand 125 psi, well within the limits of the prototype, and allowing for easier changes in configuration. Upon further consideration, a softer, flexible plumbing assembly allowed for lower weight and greater safety for the robot and was chosen for all further connections.

FIGURE 47: QUICK CONNECT UNION[71]

The valves were originally planned as mechanically operated valves, however their slow actuation time raised concerns about the ability to accurately control the fluid flow. Additionally, the mechanical valves' weight and cost made them a less attractive option. With few commercial suppliers of small solenoid valves that were not significantly over the budget, a manufacturer in China, Ningbo Yaofeng Hydraulic Electrics Company, was contacted. As it was a custom order, the lead time on the valves was almost two weeks, significantly impacting the fabrication timeline. After the valves arrived, there was very little documentation provided. This made it difficult when orienting the valves in the plumbing assembly and made testing a significantly longer process. Each valve was examined and tested in order to verify proper working condition and the configurations of the valves in on and off states. The valves were then used to determine a flow rate of the system. From this flow rate, a ⅜ in outer diameter tube was chosen. This was significantly larger than the first tubing used.

[71] (Quick Connector [Digital Image], n.d.)

FIGURE 48: SOLENOID VALVE[72]

The change in tubing required different parts, as did the change from hard to soft piping. Research was started into components that were compatible with the valves' BSP threads, the pumps NPT threads and the ⅜in (10cm) tubing quick connectors. This lead to several international part orders, significant increased cost, and a very long lead time. Finally, a tank and a one way valve were selected in order to complete the system. In all, the concept was unchanged, but the configuration went through significant restructuring.

[72] (Solenoid Irrigation Valve [Digital Image], n.d.)

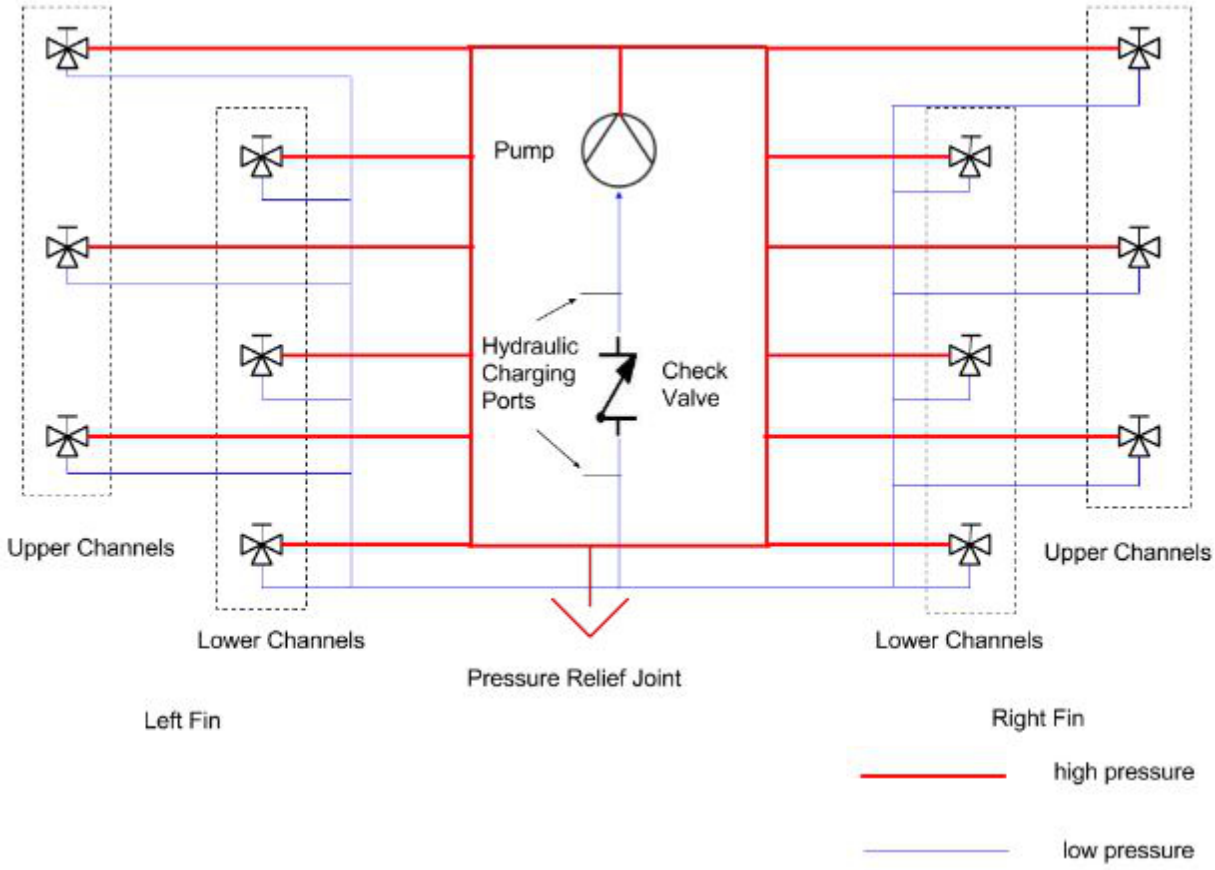

FIGURE 49: MODIFIED PLUMBING LAYOUT

After the system was set up correctly, it was verified by a pressure test. The original test resulted in significant leakage. An unaccounted for pressure release in the plastic tank caused the system to leak heavily. This problem was remedied by sealing this release with epoxy. Further testing showed no leaking.

The pump selected for the final configuration was the MG200 magnetic drive gear pump from Clark Solutions. This pump provided a significant power savings by reducing current draw to 3.4A. The pump was also considerably smaller and lighter than the Flojet pump, making integration into the hull easier. The change in pumps had no effect on the plumbing assembly layout.

Upon integration into the hull, it became clear the tank would not fit into the space allotted to the plumbing. As such, it was removed in favor of a hydraulic charging port system. This allowed air to be bled from the system without needing an additional source of hydraulic fluid.

The quick connectors proved to be difficult to work with at times, and leaked significantly during early trials. They required the mated tubes to be nearly perfectly coaxial to prevent leaking. Attempts were made to patch the leaks with silicone caulk and rubber cement, with limited success. Upon further research, it was found the tubes become worn if attached and detached from the quick connectors repeatedly. By replacing the older tubing and two failed O-rings, the leaking of the system significantly reduced. Small leaking still occurred due to the harsh angles the connectors were held at.

8.4 ECE/CS Integration

8.4.1 IMU

Upon connecting the MPU-9150 to the board, an odor and some smoke indicated that there was a short. After finding no error in how the device was wired, the breakout pins were tested with an ohm-meter. This testing revealed that three adjacent pins on the MPU were somehow shorted together within the chip. Specifically, there was no resistance between the FSYNC, AD0 and CIN pins. AD0, which had been pulled high, and FSYNC, which had been grounded, were the cause of the short. By pulling AD0 low instead of high, the last bit of the address of the device was changed from 1 to 0. This eliminated any dangerous current flow between those pins and allowed work with the chip to continue.

Promisingly, communication was established between the MPU-9150 and the MSP432. The IMU was acknowledging read and write commands, and was responding as expected to read commands. This indicated that other than the short circuit discovered, the chip was otherwise in working order. Progress stalled, however, while orientation data could not be acquired from the chip. Eventually, it was discovered that while the chip would respond to read commands properly, it would not update its registers in compliance with write commands despite acknowledging the communication. This meant that the chip could not be configured to generate the readings necessary for function and was ultimately useless.

The MPU-9150 had been discontinued by this time, so it's newer version, the MPU-9250 was acquired. Because the function of the chip was nearly identical with its previous generation, communication and configuration were easy to establish, and the chip was reporting orientation data shortly.

8.4.2 Pressure Sensor

The pressure sensor breakout board communicated with the MSP432 using I^2C. Communication had previously been successful in receiving only raw pressure values. This value does not mean much in terms of an actual measurement until the calculations are done, so the validity was confirmed against the typical value given in the data sheet.

To calculate the actual pressure in mbar based off the converted value from the breakout board's ADC, six values needed to be retrieved from the board's Programmable Read Only memory (PROM). These stored coefficients are factory calibrated values that are specific to the exact sensor on the board. Using these coefficients and the equations supplied in the data sheet, the pressure was calculated at around 9900 mbar. At the time the measurement was taken, it was compared to the barometer value at the Worcester Regional Airport, as reported by the National Weather Service. The sensor output within a reasonable variation from the reference pressure considering it was in a slightly different location.

Step	Equation	Description
1	$dT = Temp - RefTemp$	Difference between actual and reference temperature
2	$Temp = 20°C + dT * TempSense$	Actual Temperature
3	$Offset = POffset + TempPOffset * dT$	Offset at Actual Temperature
4	$Sensitivity: PSense + TempPSense * dT$	Sensitivity at Actual Temperature
5	$PFinal = Pressure * PSense - POffset$	Temperature Compensated Pressure

FIGURE 50: PRESSURE CALCULATIONS FROM DATASHEET

For easier debugging and displaying of the calculated pressure values, a Sharp Memory LCD BoosterPack was purchased. This BoosterPack is one of several that is designed to plug in directly on top of the pins on MSP launchpads. The available driver libraries make it very simple to implement. The only important change was switching the sensor code to implement I^2C on EUSCI module B1 instead of B0, because the screen communicates with the MSP432 using SPI on B0. With this simple fix, the pressure values were printed and updated regularly on the screen.

With the aid of an LCD screen, the pressure values could be seen to increase when the sensor was pressed down on. To simulate function without the actual robot, an LED was connected to another general purpose output pin on the MSP432. If the pressure value went above a certain threshold, 10000 mbar for initial testing, the theoretical robot was considered under water. In this state, the LED was off. Once the pressure was below the threshold, the LED came on as a primitive "ping" for locating and retrieving the robot in open water.

8.4.3 Electrical Connections

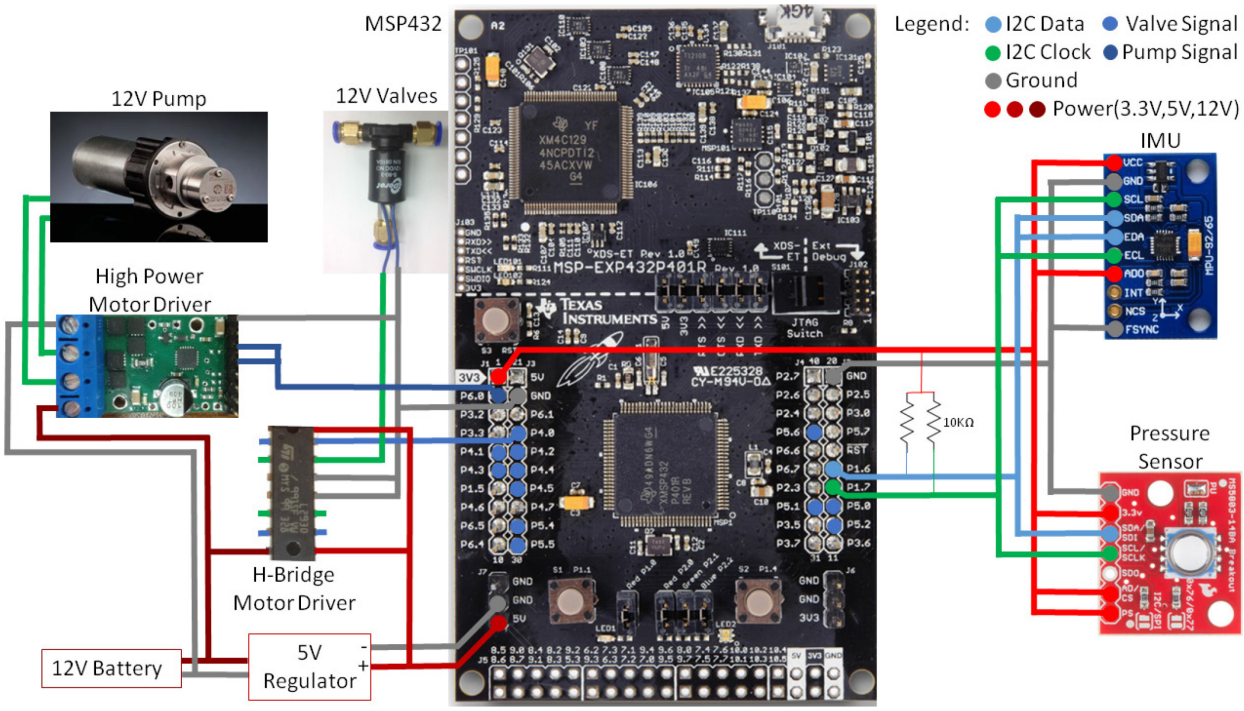

FIGURE 51: PINOUT DIAGRAM

The final pinout diagram was updated to include the high power motor driver for the pump as well as some other revised parts. In order to mimic this layout with the physical parts, several small perfboards were purchased. They came with built in buses and rails, similar to how a breadboard is laid out, to simplify soldering multiple connections to the same pin.

Sub-circuits were differentiated based on the size of the perfboards and where it was connected to the other components. The voltage regulator was placed on a perfboard with the 12V input from the battery to supply a 5V rail for the rest of the electronics. The I^2C bus was also placed on this board with different sets of rails for the data line and the clock line that both sensors could connect to.

The 5V from the board with the voltage regulator connected to the boards for the valve motor drivers. Two H-bridge motor driver chips were able to fit on one perfboard, so each fin had it's own valve control board. These were able to reach the inputs from the MSP432, 12V from the battery and the 5V from the output of the voltage regulator.

The high power motor driver connected to the pump came on its own breakout board. This board had screw terminals to connect to power, but the control lines were soldered to the standard headers to connect directly to the MSP432.

8.4.4 Code Structure

As a functional control system could not be tested before the prototype was complete, code control is largely limited to test files for different systems including fin oscillation, or gathering sensor input. Additionally, as a proof of concept for feedback-driven control, fin oscillation frequency can be controlled as a function of how far from horizontal the robot has tilted. In future control versions, putting each fin in either U or ∩ shapes would more appropriately correct the robot's roll pitch or yaw.

9.0 Results and Analysis

FIGURE 52: COMPLETED ROBOT WITH ACTUATED FINS

9.1 Project Results

The initial monetary and time budget were quite optimistic. As the fabrication process progressed, issues arose that were never even considered. Many of the issues were difficult to predict or circumvent, leading to a frustrating reworking of the initial plans on several occasions. One important lesson to take from this project is that of adding a contingency to every budget in a project. While some contingency was allowed in the project timeline for the testing and analysis, it was not nearly enough to satisfy the scope of the project. Additionally, as expected, personal funds were used to offset costs of fabrication. This removed many of the funding limits this project had, but put financial burden on the group members. A total of $600 was raised on the team website to put towards the advancement of the project. This, in addition to the WPI MQP funds, provided the majority of the required funds.

Much of the cost of the project was in research and design. This was most noticeable in the volume of silicone used for the multiple iterations of the fin fabrication process. In order to reflect the cost of the prototype, the additional costs were removed from the final project budget.

Material	Units Used	Cost per Unit	Total Cost
Dragonskin Silicone (1 gal)	2	$135.00	$270.00
Electronics Box	1	$15.00	$15.00
Acrylic Sheet	4	$20.00	$80.00
Hatch	1	$10.00	$10.00
Acrylic Cement (1 tube)	1	$10.00	$10.00
Silicone Caulk (1 tube)	1	$10.00	$10.00
4-way Quick Connector	8	$5.00	$40.00
2-way Quick Connector	14	$5.00	$70.00
Tee Quick Connector	3	$5.00	$15.00
Check Valve	1	$5.00	$5.00
Polyethylene Tubing (25ft)	1	$5.00	$5.00
3-way Solenoid Valves	12	$20.00	$240.00
Gear Pump	1	$380.00	$380.00
MSP432P401R LaunchPad	1	$20.00	$20.00
Pressure Sensor	1	$60.00	$60.00

IMU	1	$30.00	$30.00
Pump Motor Driver Circuit	1	$30.00	$30.00
Valve Motor Driver Circuit	3	$5.00	$15.00
Battery	1	$150.00	$150.00
Expenses Total:		**$1,455.00**	

FIGURE 53: PROTOTYPE MATERIAL BUDGET

9.2 Fin Results

The fin was the most critical aspect of this project, and required the most attention when evaluating the success of the prototype. It required the most innovation and adaptation of previous works to achieve. During small scale prototyping, the fin saw multiple iterations with varying degrees of success. The small scale prototyping phase was a vital step in the design process, as little documentation existed on the relationship between channel length, width and depth in relation to the motion it created. Additionally, it allowed potential issues to be identified and amended, such as the need for degassing of the silicone. Results seen in the small scale tests allowed the comparison of a multitude of designs with minimal resources invested.

The cost of the silicone proved to be the primary limiting factor when considering advancing from medium to large scale fins. The manufacturing process would have been the same as the medium scale fins, so the major hurdle would have been scale. This became significant, as it drove the hull size calculation, and meant that the medium fin would have to be redesigned to incorporate 3 channels instead of the previously planned 2.

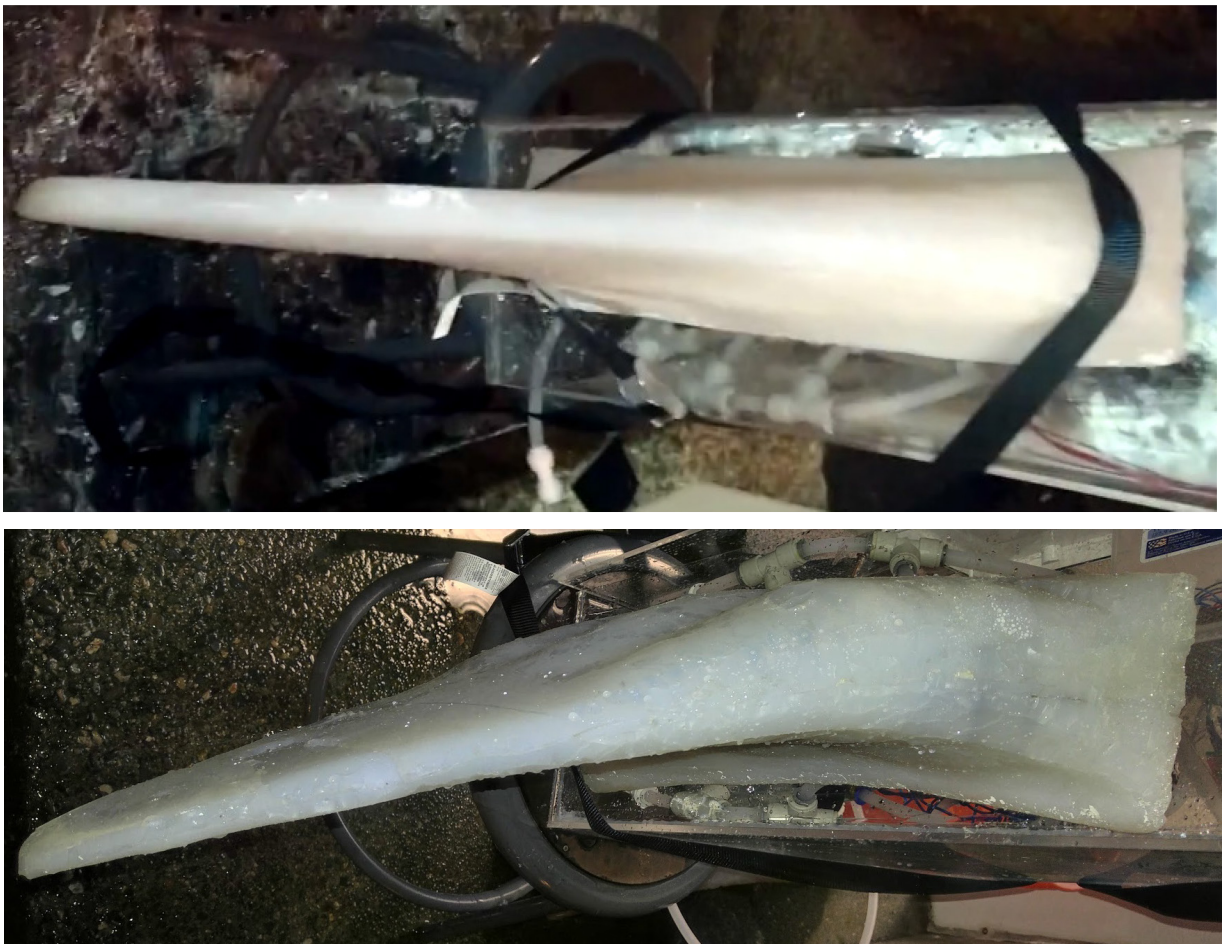

FIGURE 54: FIN ACTUATION

The set of complete fins that was created was mounted on the robot for a bench test. The fins were pressurized, then the valves started to sequence. The fins had trouble actuating upward because of their weight. To combat the issue, the robot was tilted onto the end of its hull so it would be actuating along a plane parallel to the ground. To increase the amount of actuation, all of the channels on one side were actuated at once, rather than sequenced. The fin was found to yield 60 degrees of actuation at the tip. Comparing this to our goal of 35 degrees of actuation, the fin performed greater than expected. This increase in actuation range suggests a greater value in this technology for future biomimetic robots.

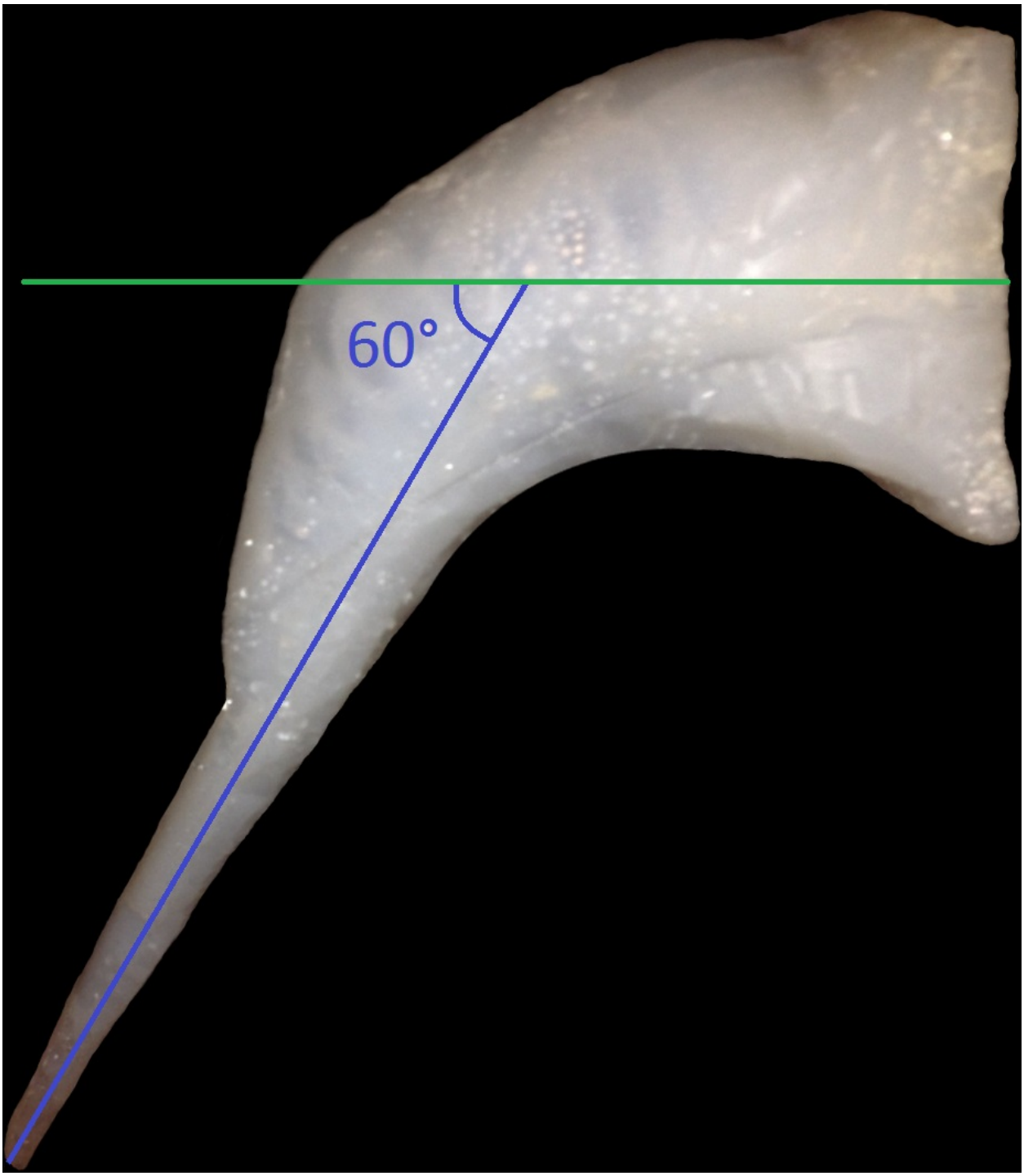

FIGURE 55: PRESSURIZED FIN WITH DEGREES OF ACTUATION

9.3 Plumbing System Results

The plumbing system required much more work than previously anticipated. The quick connectors caused significant leaking due to the tubing being pulled at harsh angles, and over used. Although the plumbing system fulfilled all its objectives, the issues with leaking took away from the ability to focus on more vital aspects of the project, and thus, would warrant a significant improvement. While flexible connectors were incredibly helpful when making modifications to the prototype, a solid plumbing system would be much more reliable.

9.4 Hull Results

While the fiberglass hull had room for significant improvement, the acrylic hull was largely successful for this prototype. It is worth noting the acrylic hull was a rectangular cube versus the smoothed body of the fiberglass hull.

The fiberglass hull ended up with many small holes as a result of the manufacturing process. Multiple attempts to seal the leaks were ultimately unsuccessful. This lead to the decision to prioritize the function of the hull over the hydrodynamic form, and switch to a simple acrylic box to house the components and support the fins.

The squared form of the new hull was not ideal from a hydrodynamic perspective, but was sufficient for the scope of this prototype. In the end, the acrylic hull was able to be successfully sealed, protecting the sensitive electronics from the outside environment.

9.5 ECE Results

Input from the sensors was communicated properly between the IMU and Pressure sensor. Signals from the MSP432 are controlling valve and pump drive as directed. Ultimately, the electrical systems were able to interface with both the mechanical systems and the code uploaded on the MSP432.

9.6 System Level Results

The integration of all the components was a challenging aspect of the project. In many cases, simply bonding surfaces together proved to be complicated processes requiring testing and multiple iterations. By scaling down the fin size, and thus the whole robot, the plumbing system was difficult to incorporate into the hull. Bonding the pressure sensor to the exterior of the hull while maintaining

waterproof rating also provided a challenge. The most surprising difficulties of this project came from interfacing between components.

FIGURE 56: COMPLETED PROTOTYPE AWAITING TESTING

10.0 Conclusions and Future Work

10.1 Conclusion

There are many approaches that can be used to develop an efficient AUV. By using biomimetic design and soft robotic actuation, it is possible to create a quiet and efficient AUV. A baseline technology was developed that has excellent potential for further development and improvement. Initial testing suggests the current prototype can perform the range of motion needed for lifelike actuation.

10.2 Future Work

Further research may include optimizing the oscillatory aspect of the fin motion. This would require additional progress in the design of the silicone fins, channel configurations, and timing of the pressurization of the channel segments. Increased accuracy could also be achieved by employing professional manufacturing methods of the mold and fin positives.

The outer covering, or “skin”, of the robot should provide optimum flow characteristics, while being flexible enough to move with the articulation of the fins. Waterproofing also stands to be a significant challenge if there will be an interface between the internal electronic systems and the exterior of the robot.

The hull is a topic for significant future work. Utilizing a production methodology that would result in an accurately fitted, waterproof hull, that also incorporates the contours and shaping for improved hydrodynamics and anatomically accurate profile.

Additional sensors and control systems could also be implemented in the future for increased control and awareness in the environment. With a functional prototype tested in the water, the control could be developed specific to the movement of the robot. This would allow for fine tuned manipulation of the fins for accurate, biomimetic motions like flapping, gliding, turning and other methods of locomotion used by manta rays. Sensors for terrain mapping and avoidance, such as sonar or a camera with image processing, would also allow for intelligent maneuvering in an environment with obstacles.

Moving forward, the team will be presenting this project at the Harvard 2016 Soft Robotics Toolkit Competition. This competition allows for greater visibility of the project, and opportunities to advance research in this topic through the Soft Robotic Toolkit’s open source documentation.

Special Thanks

The Manta Ray Robot team would like to thank the following:

- Professor Jarvis for advising the project
- Joe St. Germain for allowing access to his lab, resources, and expertise
- Professor Ludwig for allowing use of his lab space
- Marleney of WPI Facilities for all her help and encouragement

References

3-Way Mechanical Valve [Digital Image]. (n.d.). Retrieved from http://i.ebayimg.com/images/g/hZEAAOSwY45UNk8-/s-l1600.jpg

Argo Floats. (2015, Sep 18). Retrieved from http://www.argo.ucsd.edu/how_argo_floats.html

Autonomous Underwater Vehicles. (2015, Sep 18). Retrieved from WHOI.edu: http://www.whoi.edu/main/auvs

AUV Laboratory at MIT Sea Grant - Odyssey IV. (2015, Sep 18). Retrieved from MIT.edu: http://auvlab.mit.edu/vehicles/vehicle_pdfs/Odyssey_IV_spec_sheet.pdf

AUV Laboratory at MIT Sea Grant - REXII Flyer. (2015, Sep 18). Retrieved from MIT.edu: http://auvlab.mit.edu/vehicles/vehicle_pdfs/RexIIflyer.pdf

Basic Facts about Coral Reefs. (2015, Oct 17). Retrieved from http://www.defenders.org/coral-reef/basic-facts

Battery Selection. (2015, Nov). Retrieved from http://dronesarefun.com/BatteriesForUAV.html

Battery Types. (2015). Retrieved from https://www.aspectsolar.com/learn/battery-types/

BatteryTender [Digital Image]. (n.d.). Retrieved from http://www.batterytender.com/btl14a240cnt.jpg

Biomimetic. (2015, Sep 18). Retrieved from dictionary.com: http://dictionary.reference.com/browse/biomimetic

Bishop-Moser, J., Krishnan, G., Kim, C., & Kota, S. (2012). *Design of soft robotic actuators using fluid-filled fiber-reinforced elastomeric enclosures in parallel combinations.* Vilamoura: IEEE.

COHRlastic Silicone Rubber Products. (2015). Retrieved from http://www.foams.saint-gobain.com/uploadedFiles/SGfoams/Documents/COHRlastic%20Brochure.pdf

Cortex-M Series. (2015, Oct 17). Retrieved from arm.com: http://www.arm.com/products/processors/cortex-m/index.php

Dragon Skin Series. (2015, Oct 17). Retrieved from Investigating the Thrust Production of a Myliobatoid-Inspired Oscillating

Du, R., Li, Z., & Youcef-Toumi, K. V. (2015). *Robot Fish Bio-inspired Fishlike Underwater Robots.* Berlin: Springer Berlin.

Electroactive Polymer [Digital Image]. (n.d.). Retrieved from http://www3.imperial.ac.uk/pls/portallive/docs/1/66191698.JPG

Electroactive Polymers | MIT Technology Review. (2002, Jan). Retrieved from Technology Review: http://www.technologyreview.com/article/401750/electroactive-polymers/

Festo Aqua Ray. (2015, Sep 20). Retrieved from festo.com: https://www.festo.com/rep/en_corp/assets/pdf/Aqua_ray_en.pdf

Fiber-Reinforced Actuators. (2015, Oct 17). Retrieved from Soft Robitcs Toolkit: http://softroboticstoolkit.com/book/fiber-reinforced-bending-actuators

Fish, F. E., & Kocak, D. M. (2011). Biomimetics and Marine Technology: An Introduction. *Marine Technology Society Journal*, 8-13.

Flojet Pump [Digital Image[. (n.d.). Retrieved from http://ep.yimg.com/ca/I/kingpumps_2267_68453090

Garrett, S. (1998, Nov). *VEGETABLE OIL FOR LUBRICATING CHAIN SAWS* . Retrieved from http://www.fs.fed.us/t-d/pubs/html/98511316/98511316.html

Geometric Actuation [Digital Image]. (n.d.). Retrieved from http://www.bartsmithlabs.com/images/hydro-test.jpg

Hanson, J. (2005, Nov 30). *Manta Ray [Digital Image]*. Retrieved from https://commons.wikimedia.org/wiki/File:Manta_birostris-Thailand4.jpg

Harvard College. (n.d.). *PneuNet Actuator [Digital Image]*. Retrieved from http://static.projects.iq.harvard.edu/files/styles/os_files_large/public/sorotoolkit/files/fiberandstrainlayer.png?m=1395011410&itok=jMNWoVlE

http://softroboticstoolkit.com/book/pneunets-bending-actuator. (2015, Oct 17). Retrieved from http://www.engineerstudent.co.uk/pneumatics_vs_hydraulics.html

Huber, J. E., Fleck, N. A., & Ashby, M. F. (1965). The selection of mechanical actuators based on performance indices. *Proceedings Of the Royal Society A: Mathematical, Physical and Engineering Sciences*, 2185-2205.

Hydraulic System [Digital Image]. (n.d.). Retrieved from http://www.free-online-private-pilot-ground-school.com/images/hydraulic-system.gif

IMU [Digital Image]. (n.d.). Retrieved from http://www.invensense.com/products/motion-tracking/9-axis/mpu-9150/

Is water hydraulics in your future? (2015, Oct 17). Retrieved from machinedesign.com: http://machinedesign.com/archive/water-hydraulics-your-future

Lithium Battery Overview. (2015, Nov). Retrieved from https://www.batterystuff.com/kb/articles/battery-articles/lithium-battery-overview.html

Liu, G., Ren, Yan, Zhu, J., Bart-Smith, H., & Dong, H. (2015). *Thrust producing mechanisms in ray-inspired underwater vehicle propulsion.*

Maia, A. M., Wilga, C. A., & Lauder, G. V. (2012). Biomechanics of Locomotion in Sharks, Rays and Chimaeras. In J. C. Carrier, J. A. Musick, & M. R. Heithaus, *Biology of Sharks and Their Relatives, Second Edition* (pp. 125-151). CRC Press.

Manta Ray Advocates. (2016, Jan 15). Retrieved from http://www.mantarayshawaii.com/birostris.html

Mantabot [Digital Image]. (n.d.). Retrieved from http://static.ddmcdn.com/gif/robot-water-creatures-manta-ray-670.jpg

Mantabot. (2015, Sep 20). Retrieved from IEEE.org: http://spectrum.ieee.org/automaton/robotics/military-robots/mantabot

Marchese, A. D., Onal, C. D., & Rus, D. (2014). Autonomous Soft Robotic Fish Capable of Escape Maneuvers Using Fluidic Elastomer Actuators. *Soft Robotics*, 75-87.

MG200 Gear Pump [Digital Image]. (n.d.). Retrieved from http://www.clarksol.com/images/1072.jpg

Moored, K. W., Smith, W., Hester, J. M., Chang, W., & Bart-Smith, H. (n.d.). *Investigating the Thrust Production of a Myliobatoid-Inspired Oscillating.* Charlottesville: University of Virginia.

NASA Virginia Space Grant Consortium. (2015, Sep 18). Retrieved from odu.edu: http://vsgc.odu.edu/src/Conf2010/Grad%20Papers/Moored%20-%20Paper.pdf

NOAA. (2015, Aug 27). *How Deep is the Ocean?* Retrieved from NOAA: http://oceanservice.noaa.gov/facts/oceandepth.html

PneuNets Bending Actuators. (2015, Oct 17). Retrieved from Soft Robotics Toolkit: http://softroboticstoolkit.com/book/pneunets-bending-actuator

Pololu Motor Driver [Digital Image]. (n.d.). Retrieved from https://www.pololu.com/product/2992

Pressure at Depth. (n.d.). Retrieved from http://www.calctool.org/CALC/other/games/depth_press

Pressure Sensor [Digital Image]. (n.d.). Retrieved from https://learn.sparkfun.com/tutorials/ms5803-14ba-pressure-sensor-hookup-guide

Quick Connector [Digital Image]. (n.d.). Retrieved from http://www.gamurdock.com/gam/images/products/zoom/unionconnect.jpg

RiSE Project. (2015, Sep 18). Retrieved from UPenn.edu: http://kodlab.seas.upenn.edu/~rise/newsite/index.php?leaf=1

Serpentine Wire Mechanism [Digital Image]. (n.d.). Retrieved from http://www.ipe.cuhk.edu.hk/projects23_files/Serpentine_Wire_driven_Mechanism.png

Solenoid Irrigation 3-Way Valve. (n.d.). Retrieved from http://solenoid.en.alibaba.com/product/60018396845-200200013/water_underground_drip_irrigation_3_way_solenoid_valve_12v.html?spm=a2700.7803228.1998738836.11.DN6kyD

Solenoid Irrigation Valve [Digital Image]. (n.d.). Retrieved from http://www.alibaba.com/product-detail/1-8-landscape-irrigation-laching-Pulse_60332221422/showimage.html

The difference between car and boat batteries. (2015, Oct 17). Retrieved from http://www.theglobeandmail.com/globe-drive/culture/commuting/the-difference-between-car-and-boat-batteries/article1372050/

TI LaunchPad. (2015, Sep 18). Retrieved from Texas Instruments: http://www.ti.com/ww/en/launchpad/launchpads-msp430-msp-exp432p401r.html

Water Hydraulics: Benefits and Limitations. (2015, Dec 28). Retrieved from http://hydraulicspneumatics.com/200/TechZone/HydraulicFluids/Article/False/6452/TechZone-HydraulicFluids

What is the difference between a normal lead-acid car battery and a deep cycle battery? (2015, Oct 17). Retrieved from How Stuff Works: http://auto.howstuffworks.com/question219.htm

Zhou, C., & Low, K. H. (2011). Design and Locomotion Control of a Biomimetic Underwater Vehicle With Fin Propulsion. *IEEE/ASME Transactions on Mechatronics*, 25-35.